21 Scattering and Diffraction

The solution of this problem presents mathematical difficulties which arise from the necessity of taking into account the geometrical shape of the obstacles on which the wave is falling.
Vladimir Fock (1948)

21.1 Introduction

An incident electromagnetic wave is said to *scatter* or *diffract* from a sample of matter when the field produced by the sample *cannot* be described using Fresnel's theory of reflection and refraction from a flat interface (Section 17.3). In this chapter, we focus on the class of problems where this occurs because the wavelength of the incident monochromatic field is *not small* compared to the curvature of a material boundary. From a Fresnel point of view, the total field in these cases results from the interference of many different "reflected" and "refracted" waves propagating in different directions. We will encounter other points of view as we proceed. Figure 21.1 shows some typical geometries of interest. There is no universal naming practice, but many authors say that "scattering" occurs from objects with smooth boundaries and "diffraction" occurs from objects with sharp edges.

The physics which produces scattering and diffraction is identical to the physics which produces the Fresnel equations. An incident electromagnetic wave sets the charged particles of a medium into motion. Each accelerated charge produces a retarded field which is felt by, and thus affects the motion of, every other charge in the medium. The motion of every charge and the field it produces must be consistent with the total field each charge experiences. The sum of the fields produced by all the particles of the medium is called the "scattered field" and the total field at any point (inside or outside the object) is the sum of the incident field and the scattered field:

$$\mathbf{E} = \mathbf{E}_{\text{inc}} + \mathbf{E}_{\text{scatt}}. \tag{21.1}$$

The same phenomenon viewed from a macroscopic perspective treats the moving charged particles as an induced current. This current is the source of $\mathbf{E}_{\text{scatt}}$. Bearing in mind the constitutive relation of the matter, the actual current density is the one which ensures that (21.1) satisfies the boundary (or matching) condition at the surface of the scattering medium. The complexities of the problem all arise from the shape of the scatterer.

The proper treatment of scattering and diffraction has consistently attracted the attention of mathematical physicists of the first rank. The names Fresnel, Helmholtz, Rayleigh, and Kirchhoff are closely associated with a scalar theory developed for acoustics and optics. After Maxwell folded optics into electromagnetism, vector field calculations of lasting influence were performed by Debye, Mie, and Sommerfeld. The problems of radar engaged the quantum pioneers Fock and Schwinger, both of whom made profound contributions to the classical theory of electromagnetic scattering and diffraction. New insights appear today in contexts as diverse as the rainbow, laser propagation, and near-field microscopy.

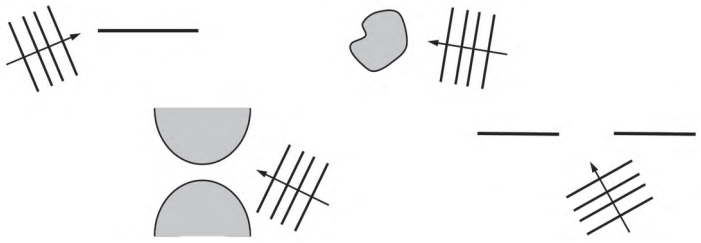

Figure 21.1: Four situations where a plane wave approaches an object with a sharp edge or a surface curvature which is large compared to the incident wavelength. Figure adapted from Toraldo di Francia (1953).

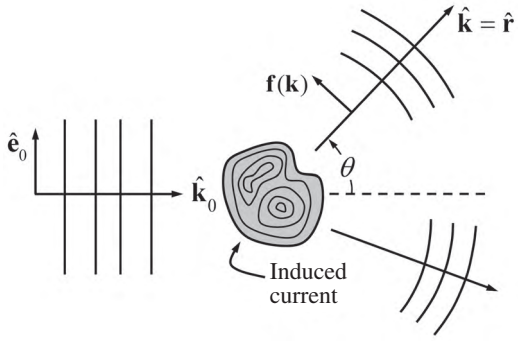

Figure 21.2: A plane wave with polarization vector $\hat{\mathbf{e}}_0$ propagating in the $\hat{\mathbf{k}}_0$ direction induces currents in a sample of matter. The scattering amplitude $\mathbf{f}(\mathbf{k})$ transverse to the local plane wave propagation direction $\hat{\mathbf{k}}$ characterizes the strength of the field radiated in that direction.

The diversity of scattering and diffraction problems, and the diversity of the mathematical techniques developed to treat them, is very great. For that reason, the aim of this chapter is less to teach quantitative scattering theory than to expose the reader to some of the basic ideas and to present a selection of representative results. To that end, we begin with scattering from small objects and thereby make immediate contact with the theory of electric and magnetic dipole radiation. Higher-order contributions become increasingly important as the size of the scattering object increases and an exact partial wave analysis is possible for cylinders and spheres. Most real scattering problems cannot be solved exactly, so we describe the Born and physical optics approximations as examples of what can be done without extensive numerical work. Our approach to diffraction focuses on the classic problem of a plane wave incident on an aperture in a plane screen. This leads us to discuss the electromagnetic version of optical principles like Huygens' principle and Babinet's principle. The example of wave transmission through a sub-wavelength aperture serves to demonstrate that scattering and diffraction are far from exhausted as topics for contemporary research.

21.2 The Scattering Cross Section

The cartoon in Figure 21.2 shows a conducting or dielectric object which scatters an incident plane wave with polarization vector $\hat{\mathbf{e}}_0$ and propagation vector $\hat{\mathbf{k}}_0$. The figure of merit for this process is called the *differential cross section* for scattering. Up to a factor of r^2, this is the radial component of

the time-averaged Poynting vector of the radiation field $\mathbf{E}_{\text{rad}}$ (the long-distance part of $\mathbf{E}_{\text{scatt}}$) divided by the magnitude of the time-averaged Poynting vector of the incident field $\mathbf{E}_{\text{inc}}$:

$$\frac{d\sigma_{\text{scatt}}}{d\Omega} = \frac{\text{scattered power radiated into a unit solid angle}}{\text{incident power per unit area}} = \frac{r^2\hat{\mathbf{r}}\cdot\langle\mathbf{S}_{\text{rad}}\rangle}{|\langle\mathbf{S}_{\text{inc}}\rangle|}. \tag{21.2}$$

A convenient form for (21.2) follows from the general characteristics of $\mathbf{E}_{\text{rad}}$ outlined in Section 20.5 for a compact, three-dimensional, time-harmonic source. First, it is an outgoing spherical wave with radial dependence $\exp(ikr)/r$. Second, the spherical wave front flattens out (locally) into a plane wave front with propagation vector $\mathbf{k} = k\hat{\mathbf{r}}$. Third, the field direction is transverse to the propagation direction. A *scattering amplitude* $\mathbf{f}(\mathbf{k}) \perp \mathbf{k}$ is commonly used to describe the vector and angular behavior of the scattered radiation field. Combining all this information permits us to write the asymptotic ($r \to \infty$) total field (21.1) in the form

$$\lim_{r\to\infty}\mathbf{E} = \mathbf{E}_{\text{inc}} + \mathbf{E}_{\text{rad}} = E_0\left[\hat{\mathbf{e}}_0 e^{i\mathbf{k}_0\cdot\mathbf{r}} + \frac{e^{ikr}}{r}\mathbf{f}(\mathbf{k})\right]e^{-i\omega t}. \tag{21.3}$$

All the wave fields in (21.3) propagate in vacuum, so $k = k_0 = \omega/c$.

Comparing (21.2) with (20.81) shows that the differential cross section is a normalized version of the time-averaged angular distribution of radiated power. Making use of (20.120) and (21.3),

$$\frac{d\sigma_{\text{scatt}}}{d\Omega} = \frac{\langle dP/d\Omega\rangle}{\frac{1}{2}\epsilon_0 c E_0^2} = r^2\frac{|\mathbf{E}_{\text{rad}}|^2}{|\mathbf{E}_0|^2} = |\mathbf{f}(\mathbf{k})|^2. \tag{21.4}$$

If our interest is a scattered electric field with a particular polarization $\boldsymbol{\epsilon}$, (21.4) generalizes to[1]

$$\left.\frac{d\sigma_{\text{scatt}}}{d\Omega}\right|_{\boldsymbol{\epsilon}} = r^2\frac{|\boldsymbol{\epsilon}^*\cdot\mathbf{E}_{\text{rad}}|^2}{|\mathbf{E}_0|^2} = |\boldsymbol{\epsilon}^*\cdot\mathbf{f}(\mathbf{k})|^2. \tag{21.5}$$

The results of Section 20.5.6 relate $\mathbf{E}_{\text{rad}}$ to the time-harmonic current density $\mathbf{j}(\mathbf{r}|\omega)\exp(-i\omega t)$ induced in the scatterer by the incident field:

$$\mathbf{E}_{\text{rad}} = -\frac{ik}{4\pi\epsilon_0 c}\hat{\mathbf{k}}\times\left[\hat{\mathbf{k}}\times\int d^3r'\,\mathbf{j}(\mathbf{r}'|\omega)\exp(-i\mathbf{k}\cdot\mathbf{r}')\right]\frac{\exp[i(kr-\omega t)]}{r}. \tag{21.6}$$

Then, because $|\hat{\mathbf{k}}\times\hat{\mathbf{k}}\times\mathbf{v}|^2 = |\hat{\mathbf{k}}\times\mathbf{v}|^2$ for any vector $\mathbf{v}$, substituting (21.6) into (21.4) gives

$$\frac{d\sigma_{\text{scatt}}}{d\Omega} = \left(\frac{k}{4\pi\epsilon_0 E_0 c}\right)^2\left|\hat{\mathbf{k}}\times\int d^3r'\,\mathbf{j}(\mathbf{r}'|\omega)\exp(-i\mathbf{k}\cdot\mathbf{r}')\right|^2. \tag{21.7}$$

The integral over all space of the differential cross section is called the *total cross section* for scattering:

$$\sigma_{\text{scatt}} = \int d\Omega\frac{d\sigma_{\text{scatt}}}{d\Omega}. \tag{21.8}$$

The dimensions of σ_{scatt} are length squared, which makes it convenient to compare (21.8) with the geometric cross section, σ_{geom}, defined as the projected area of the scattering object intercepted by the incident plane wave.

21.3 Thomson Scattering

Thomson scattering occurs when an electromagnetic plane wave interacts with a single free electron. Classically, we model the electron as a point particle with charge $-e$ and mass m which responds

[1] Let $\boldsymbol{\epsilon}_k$ be a complete set of polarization vectors. Then $|\mathbf{E}_{\text{rad}}|^2 = |\sum_k(\boldsymbol{\epsilon}_k^*\cdot\mathbf{E}_{\text{rad}})\boldsymbol{\epsilon}|^2 = \sum_k|\boldsymbol{\epsilon}_k^*\cdot\mathbf{E}_{\text{rad}}|^2$.

to $\mathbf{E}_{\rm inc} = \hat{\mathbf{e}}_0 E_0 \exp[i(\mathbf{k}_0 \cdot \mathbf{r} - \omega t)]$ and $c\mathbf{B}_{\rm inc} = \hat{\mathbf{k}}_0 \times \mathbf{E}_{\rm inc}$. We showed in Section 16.10.1 that the magnetic Lorentz force may be neglected compared to the electric Coulomb force when the field strength is weak. Therefore, with $\hat{\mathbf{e}}_0 \parallel \hat{\mathbf{z}}$, the equation of motion for the trajectory $\mathbf{r}_0(t)$ of the electron is

$$m\ddot{\mathbf{r}}_0 = -eE_0 \exp[i(\mathbf{k}_0 \cdot \mathbf{r}_0 - \omega t)]\hat{\mathbf{e}}_0. \tag{21.9}$$

This motion produces the time-harmonic current density

$$\mathbf{j}(\mathbf{r}, t) = -e\dot{z}_0(t)\delta(\mathbf{r} - \mathbf{r}_0)\hat{\mathbf{e}}_0 = \frac{ie^2 E_0}{m\omega} \exp[i(\mathbf{k}_0 \cdot \mathbf{r}_0 - \omega t)]\delta(\mathbf{r} - \mathbf{r}_0)\hat{\mathbf{e}}_0. \tag{21.10}$$

Because $\hat{\mathbf{e}}_0 \cdot \hat{\mathbf{e}}_0^* = 1$, using (21.10) with $\mathbf{r}_0 = 0$ to evaluate (21.7) gives the Thomson scattering cross section,[2]

$$\frac{d\sigma_{\rm Thom}}{d\Omega} = \left(\frac{e^2}{4\pi\epsilon_0 mc^2}\right)^2 |\hat{\mathbf{k}} \times \hat{\mathbf{e}}_0|^2 \equiv r_e^2 \left(1 - |\hat{\mathbf{k}} \cdot \hat{\mathbf{e}}_0|^2\right). \tag{21.11}$$

This formula is valid for all choices of $\hat{\mathbf{e}}_0$, whether real (for linear polarization) or complex (for circular or elliptical polarization).

The magnitude of the frequency-independent Thomson cross section is set by a length called the *classical electron radius*,

$$r_e = \frac{e^2}{4\pi\epsilon_0 mc^2} \approx 2.82 \times 10^{-15} \text{ m}. \tag{21.12}$$

This is the radius of a charged sphere whose Coulomb self-energy is equal to the rest energy of the electron. Alternately, $r_e = \alpha\lambda_c = \alpha^2 a_{\rm B}$, where $a_{\rm B} \approx 5.3 \times 10^{-11}$ m is the Bohr radius, $\alpha \approx 1/137$ is the fine structure constant, and $\lambda_c = \alpha a_{\rm B}$ is the Compton wavelength of the electron.

The absence of scattering along the direction of the electric field ($\mathbf{k} \parallel \hat{\mathbf{e}}_0$) and the angular dependence of (21.11) are reminiscent of the behavior of dipole radiation shown in Figure 20.17 of Section 20.7.1. This is not an accident. From (21.10), the motion of the oscillating point charge produces an electric dipole moment,

$$\mathbf{p}(t) = -ez(t) = -\frac{e^2 E_0}{m\omega^2}\hat{\mathbf{e}}_0 \exp(-i\omega t) = \mathbf{p} \exp(-i\omega t), \tag{21.13}$$

which in turn produces an electric dipole radiation field (20.160),

$$\mathbf{E}_{\rm rad} = -\frac{\mu_0}{4\pi}\omega^2[\hat{\mathbf{k}} \times (\hat{\mathbf{k}} \times \mathbf{p})]\frac{e^{i(kr-\omega t)}}{r}. \tag{21.14}$$

Comparing (21.14) to (21.3) gives $\mathbf{f} = (\mu_0 e^2/4\pi m)[\hat{\mathbf{e}}_0 - (\hat{\mathbf{k}} \cdot \hat{\mathbf{e}}_0)\hat{\mathbf{k}}]$, and inserting this into the far right-hand side of (21.4) reproduces the Thomson cross section (21.11).

It is useful to introduce the coordinate system shown in Figure 21.3 where $\hat{\mathbf{e}}_1 = \hat{\mathbf{e}}_\perp$ and $\hat{\mathbf{e}}_2 = \hat{\mathbf{e}}_\parallel$ are orthogonal unit vectors which lie perpendicular and parallel to the *scattering plane* defined by $\hat{\mathbf{k}}_0$ and $\hat{\mathbf{k}}$. For example, suppose we substitute first $\mathbf{p} = p\hat{\mathbf{e}}_\perp$ and then $\mathbf{p} = p\hat{\mathbf{e}}_\parallel$ into (21.14). Using Figure 21.3, we deduce that $\mathbf{E}_{\rm rad}$ shares the polarization of the incident wave in the sense of being polarized either perpendicular or parallel to the scattering plane.

Equation (21.11) is the cross section for scattering when the incident plane wave has fixed polarization $\hat{\mathbf{e}}_0$. To find the cross section for an *unpolarized* incident wave (a random mixture of waves with

[2] The time-independent choice $\mathbf{r}_0 = 0$ implies that the displacement of the electron away from the origin may be neglected in (21.7). This is a long-wavelength, low-velocity approximation.

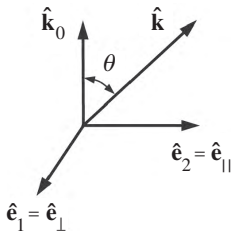

Figure 21.3: Orthogonal linear polarization vectors $\hat{\mathbf{e}}_1$ and $\hat{\mathbf{e}}_2$. The latter lies in the scattering plane defined by $\mathbf{k}_0$ and $\mathbf{k}$.

any two orthogonal polarization vectors, $\hat{\mathbf{e}}_1$ and $\hat{\mathbf{e}}_2$), we perform a statistical average of (21.11) over the two polarizations:

$$\left.\frac{d\sigma_{\text{Thom}}}{d\Omega}\right|_{\text{unpol}} = \frac{1}{2}\sum_{m=1}^{2} r_e^2(1 - |\hat{\mathbf{k}} \cdot \hat{\mathbf{e}}_m|^2). \tag{21.15}$$

Using the polarization vectors defined in Figure 21.3 to evaluate the contributions to (21.15), we find immediately that

$$\frac{d\sigma_\perp}{d\Omega} = r_e^2 \qquad \text{and} \qquad \frac{d\sigma_\parallel}{d\Omega} = r_e^2 \cos^2\theta. \tag{21.16}$$

Therefore,

$$\left.\frac{d\sigma_{\text{Thom}}}{d\Omega}\right|_{\text{unpol}} = \frac{1}{2}\left[\frac{d\sigma_\perp}{d\Omega} + \frac{d\sigma_\parallel}{d\Omega}\right] = \frac{1}{2} r_e^2 \left(1 + \cos^2\theta\right). \tag{21.17}$$

Unlike (21.11), the cross section (21.17) for scattering unpolarized waves is non-zero at every scattering angle. The total *Thomson cross section* is the integral of (21.17) over all these angles:

$$\sigma_{\text{Thom}} = \int d\Omega \left.\frac{d\sigma_{\text{Thom}}}{d\Omega}\right|_{\text{unpol}} = \frac{8\pi}{3} r_e^2. \tag{21.18}$$

The information in (21.16) also leads naturally to a definition for the *degree of polarization* of the scattered radiation. This is

$$\Pi(\theta) = \frac{\dfrac{d\sigma_\perp}{d\Omega} - \dfrac{d\sigma_\parallel}{d\Omega}}{\dfrac{d\sigma_\perp}{d\Omega} + \dfrac{d\sigma_\parallel}{d\Omega}} = \frac{\sin^2\theta}{1 + \cos^2\theta}. \tag{21.19}$$

The plots of (21.17) and (21.19) in Figure 21.4 show that the electric dipole scattering of unpolarized waves peaks in the forward ($\theta = 0$) and backward ($\theta = \pi$) directions and that the radiation is 100% linearly polarized for scattering at right angles ($\theta = \pi/2$) to the direction of incidence.

Example 21.1 Evaluate (21.15) in a coordinate-system-independent way using the fact that $\hat{\mathbf{e}}_1$, $\hat{\mathbf{e}}_2$, and $\hat{\mathbf{k}}_0$ form an orthonormal triad [see (16.48)].

Solution: The stated information means that the vectors in question satisfy a completeness relation. We write the latter in both abstract and component form as

$$|\hat{\mathbf{e}}_1\rangle\langle\hat{\mathbf{e}}_1| + |\hat{\mathbf{e}}_2\rangle\langle\hat{\mathbf{e}}_2| + |\hat{\mathbf{k}}_0\rangle\langle\hat{\mathbf{k}}_0| = 1 \qquad \text{or} \qquad \hat{e}_{1i}\hat{e}^*_{1j} + \hat{e}_{2i}\hat{e}^*_{2j} + \hat{k}_{0i}\hat{k}_{0j} = \delta_{ij}.$$

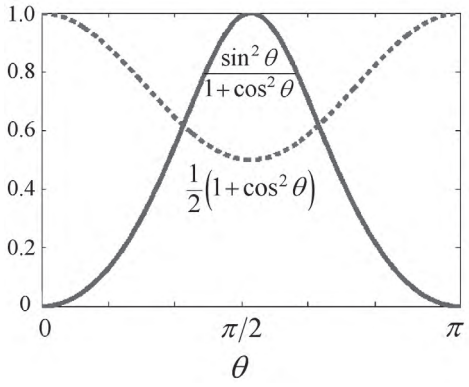

Figure 21.4: Angular dependence of the cross section (dashed curve) and degree of polarization (solid curve) for Thomson (and Rayleigh) scattering.

Using the second of these,

$$\sum_{m=1}^{2} |\hat{\mathbf{k}} \cdot \hat{\mathbf{e}}_m|^2 = \hat{k}_i \hat{k}_j \hat{e}_{mi} \hat{e}^*_{mj} = \hat{k}_i \hat{k}_j \left(\delta_{ij} - \hat{k}_{0i} \hat{k}_{0j}\right) = 1 - (\hat{k} \cdot \hat{k}_0)^2.$$

Therefore, because $\hat{\mathbf{k}}_0 \cdot \hat{\mathbf{k}} = \cos\theta$, (21.15) becomes

$$\left.\frac{d\sigma_{\text{Thom}}}{d\Omega}\right|_{\text{unpol}} = \frac{1}{2} r_e^2 \left[2 - \left(1 - \cos^2\theta\right)\right] = \frac{1}{2} r_e^2 \left(1 + \cos^2\theta\right).$$

Example 21.2 Show that the cross section for monochromatic plane wave scattering from a collection of N electrons with fixed positions $\mathbf{r}_k$ is proportional to the absolute square of the spatial Fourier transform of the electron density $n(\mathbf{r}) = \sum_{k=1}^{N} \delta(\mathbf{r} - \mathbf{r}_k)$.

Solution: In the presence of a time-harmonic plane wave, the current density for all N electron is the sum of terms like (21.10), except that the particles are located at positions $\mathbf{r}_k$ rather than at the origin. The space part of this density is

$$\mathbf{j}(\mathbf{r}|\omega) = -\frac{ie^2 E_0}{m\omega} \exp(i\mathbf{k}_0 \cdot \mathbf{r}) \hat{\mathbf{e}}_0 \sum_{k=1}^{N} \delta(\mathbf{r} - \mathbf{r}_k).$$

Substituting the foregoing into (21.7) shows that the cross section for scattering from the electron ensemble is proportional to the cross section for scattering from a single electron:

$$\left.\frac{d\sigma}{d\Omega}\right|_{\text{ensemble}} = \frac{d\sigma_{\text{Thom}}}{d\Omega} \times \left| \sum_{k=1}^{N} \exp[i(\mathbf{k}_0 - \mathbf{k}) \cdot \mathbf{r}_k] \right|^2.$$

On the other hand, the Fourier transform of the electron density is

$$n(\mathbf{q}) = \int d^3 r\, n(\mathbf{r}) \exp(-i\mathbf{q} \cdot \mathbf{r}) = \sum_{k=1}^{N} \int d^3 r\, \delta(\mathbf{r} - \mathbf{r}_k) \exp(-i\mathbf{q} \cdot \mathbf{r})$$

$$= \sum_{k=1}^{N} \exp(-i\mathbf{q} \cdot \mathbf{r}_k) = n^*(-\mathbf{q}).$$

If we define a *scattering wave vector* $\mathbf{q} = \mathbf{k_0} - \mathbf{k}$, the two preceding equations give the advertised result:

$$\left.\frac{d\sigma}{d\Omega}\right|_{\text{ensemble}} = \frac{d\sigma_{\text{Thom}}}{d\Omega} \times |n(\mathbf{q})|^2 = \frac{d\sigma_{\text{Thom}}}{d\Omega} \times \sum_{k=1}^{N}\sum_{j=1}^{N} \exp[i\mathbf{q}\cdot(\mathbf{r}_k - \mathbf{r}_j)].$$

This cross section formula underpins the theory of X-ray scattering, and the double sum is called a *form factor* in that context. X-ray scattering is sensibly regarded as an energy-conserving, elastic process for valence electrons whose binding energies are small compared to the energy of an incident X-ray. This implies that $|\mathbf{k}_0| = |\mathbf{k}|$, in which case Figure 21.2 shows that $q = 2k\sin(\frac{1}{2}\theta)$.

Application 21.1 The Polarization of Cosmic Microwave Radiation

Figure 16.5 shows that the background microwave radiation received from the cosmos is linearly polarized. The origin of this polarization is Thomson scattering and a small spatial anisotropy in the temperature of the radiation itself. The cartoons in Figure 21.5 tell the story by focusing on the radiation seen by an observer on the positive z-axis. Figure 21.5(a) shows linearly polarized plane waves incident on an electron at the origin from the $\pm x$ and $\pm y$ directions. Because Thomson scattering preserves polarization and is maximal at right angles to the incident wave polarization (see Figure 20.17), the waves incident from the $\pm x$ directions scatter into y-polarized waves on the z-axis and the waves incident from the $\pm y$ directions scatter into x-polarized waves on the z-axis. Thus, the observed radiation is unpolarized. This conclusion does not change if we add incoming z-polarized waves from the $\pm x$ and $\pm y$ directions (so all the incident radiation is unpolarized) because their cross section for scattering into the z-direction is zero.

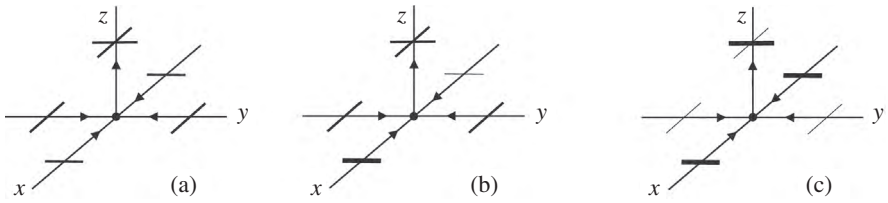

Figure 21.5: Cartoon of linearly polarized planes waves incident from $\pm x$ and $\pm y$ which scatter from an electron at the origin into the $+z$-direction of observation. The horizontal bars indicate the direction of polarization of each wave. The thickness of the bars indicates the intensity of the wave. The spatial distribution of the incident wave intensity is (a) isotropic; (b) dipole anisotropic; and (c) quadrupole anisotropic. The observed radiation is (a) unpolarized; (b) unpolarized; and (c) linearly polarized. Figure adapted from Dodelson (2003). Copyright Elsevier 2003.

Figure 21.5(b) introduces a dipole anisotropy by making the wave amplitude bigger (smaller) than the average for plane waves incident from the $+x$ $(-x)$ direction. A dipole anisotropy in the blackbody radiation temperature would have this effect. There is no change in the unpolarized radiation observed on the z-axis because the altered waves scatter into the $+z$-direction (preserving both polarization and amplitude) and simply superpose to give y-polarized waves on the z-axis with the average intensity of the waves scattered from the $\pm y$-axes. Finally, Figure 21.5(c) introduces a quadrupole anisotropy by making the wave amplitude bigger (smaller) than the average for plane waves incident from the $\pm x$ $(\pm y)$ directions. This produces the desired result: a net linear polarization of the waves scattered into the direction of the observer. This is consistent with independent measurements which confirm that the large-scale spatial isotropy of the blackbody temperature of the microwave radiation is perturbed by a small quadrupole anisotropy. ■

21.4 Rayleigh Scattering

Rayleigh scattering occurs when an electromagnetic plane wave impinges on a small dielectric or conducting object. By small, we mean that all characteristic linear dimensions of the object are small compared to the wavelength $\lambda = 2\pi/k_0$ of the plane wave. Under these conditions, we showed in Section 20.7 that the first few terms of a Cartesian multipole expansion of the radiation fields are sufficient to extract the physics. The incident **E** and **B** fields are nearly constant over the object's volume and the far-zone field is dominated by the radiation produced by the time-harmonic electric and magnetic dipole moments induced in the object. We compute the cross section from (21.4) by adding the magnetic dipole electric field (20.176) to the electric dipole electric field (21.14):

$$\frac{d\sigma_{\text{Ray}}}{d\Omega} = \left(\frac{k_0^2}{4\pi\epsilon_0 E_0 c}\right)^2 \left|\hat{\mathbf{k}} \times \mathbf{m} + \hat{\mathbf{k}} \times (\hat{\mathbf{k}} \times c\mathbf{p})\right|^2 . \tag{21.20}$$

Let a be the largest linear dimension of the scattering object. The condition $k_0 a \ll 1$ implies that the plane wave fields are nearly uniform over its volume and a quasistatic approximation is sufficient to calculate the induced moment(s). The simplest example is a non-magnetic dielectric object with electric polarizability α where the electric dipole moment is

$$\mathbf{p} = \alpha\epsilon_0 E_0 \hat{\mathbf{e}}_0. \tag{21.21}$$

The corresponding cross section is

$$\frac{d\sigma_{\text{Ray}}}{d\Omega} = \left(\frac{k_0^2\alpha}{4\pi}\right)^2 \left(1 - |\hat{\mathbf{k}} \cdot \hat{\mathbf{e}}_0|^2\right). \tag{21.22}$$

On dimensional grounds alone, the polarizability scales with the object volume, which is of the order of a^3. Therefore, the total Rayleigh scattering cross section, σ_{Ray}, obtained by integrating (21.22) over all angles, is much smaller that the geometric cross section of the object:

$$\sigma_{\text{Ray}} \sim a^2 (k_0 a)^4 \ll a^2. \tag{21.23}$$

The electric dipole Rayleigh cross section (21.22) and the Thomson cross section (21.11) have exactly the same angular dependence. Therefore, the discussion leading to the $1 + \cos^2\theta$ dependence in (21.20) for an unpolarized incident wave remains valid for electric dipole Rayleigh scattering. The same is true for the discussion leading to the degree of polarization (21.19). This means that Figure 21.4 applies to Rayleigh scattering as well as to Thomson scattering. Indeed, the strong linear polarization observed for skylight is a powerful indicator that dipole scattering dominates the interaction of the Sun's rays with the atmosphere.

21.4.1 Atmospheric Color

The striking λ^{-4} dependence of (21.22) is the origin of the blue color of the daylight sky and the red color of the setting Sun.[3] Looking away from the Sun during the day, we see sunlight scattered into our eyes by the molecules of the atmosphere. Because $\lambda_{\text{blue}} < \lambda_{\text{red}}$, (21.23) implies that blue light is the dominant component of the scattered light. We see red light looking directly at the Sun at sunset because the blue light has been scattered out of our line of sight. This argument is appealing precisely because it is so simple. On the other hand, it glosses over some subtleties.[4]

One subtlety is that the incoherent scattering argument presented above is not obviously relevant when (as is usual) $N \gg 1$ molecules lie inside a typical volume $V \sim \lambda^3$ of the visible sky. It could be

[3] See the cover of this volume.
[4] See Sources, References, and Additional Reading for more details.

that destructive interference wipes out the incoherent scattering intensity altogether. A proper coherent calculation requires that we perform the double sum over N quoted at the end of Example 21.2. There are two ways to do this, provided some information is supplied about the spatial correlations of the molecules within the volume. The first method (due to Rayleigh) is a brute-force sum over the molecular positions in V. The second method (due to Smoluchowski and Einstein) divides V into smaller sub-volumes and rearranges the sum to show that fluctuations (deviations) from the mean number of molecules in each sub-volume are essential to avoid destructive interference. The two methods are equivalent and give the same answer, namely, that the incoherent scattered intensity survives: the scattering intensity from all the molecules in V is simply N times the scattering intensity from a single molecule.

Another subtlety is that the Sun radiates as a $T = 6000\,\mathrm{K}$ blackbody with a spectral radiance which decreases with wavelength in the visible.[5] Under these conditions, the λ^{-4} argument more naturally predicts a violet sky than a blue sky. This is not what you see because the human brain assigns a color to incoming light based on the stimulus it receives from photoreceptive cells in the eye called cones. It happens that there are three types of cones, each with its own sensitivity to different visible wavelengths. An average observer reports that the daylight sky is blue because that color (rather than violet) represents the combined response of all three cone types to the spectral radiance of the Sun weighted by the Rayleigh λ^{-4} factor.

21.5 Two Exactly Solvable Problems

The scattering cross section can be computed exactly for objects with very simple shapes. In this section, we derive the exact cross section for scattering from a *conducting cylinder* and discuss the exact cross section for scattering from a *dielectric sphere*. We do this (i) to discover some generic features of scattering from extended distributions of matter; (ii) for later use in assessing the quality of approximate calculations; and (iii) because cylinders and spheres are good models for wires and raindrops (among other things).

The calculations are possible because a plane wave can be expressed as a sum of elementary solutions of the Helmholtz equation with either cylindrical or spherical symmetry. If the scattered field (produced by the object) is written as a similar sum with unknown expansion coefficients, the coefficients can be determined from the condition that the total field satisfies appropriate boundary or matching conditions at the surface of the object. The final solutions take the form of infinite sums of special functions which are amenable to numerical evaluation and thus to the identification of trends over large ranges of the parameters. Special analytic techniques valid for limited ranges of the parameters provide insight into the mechanisms of scattering. Indeed, the latter are practically essential for interpreting the results of numerical scattering calculations for both conducting and dielectric bodies.

21.5.1 Scattering from a Conducting Cylinder

Figure 21.6 shows a plane wave propagating in the $+x$-direction toward a perfectly conducting cylinder of radius a aligned with the z-axis. The polarization (electric field) vector lies in the y-z plane and it is sufficient to compute the scattered field separately for $\mathbf{E} \parallel \hat{\mathbf{z}}$ and $\mathbf{E} \perp \hat{\mathbf{z}}$. The results for these two cases can be superposed to treat the general case. Polarization parallel to the cylinder axis induces surface currents in the $\hat{\mathbf{z}}$-direction only. The associated vector potential points along $\hat{\mathbf{z}}$ also, so $B_z = (\nabla \times \mathbf{A})_z = 0$. On the other hand, $E_z = -\partial_z \varphi - \partial_t A_z \neq 0$. This is the only field component needed because $cB_\phi = -E_z$ in the radiation zone where the cross section is defined. Polarization

[5] Figure 19.19 is a graph of spectral radiance $T = 2.73\,\mathrm{K}$.

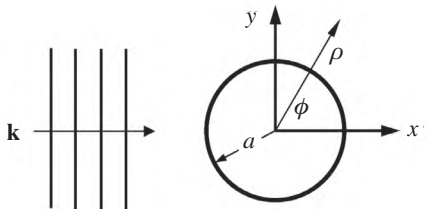

Figure 21.6: A plane wave approaches an infinite cylinder at normal incidence.

perpendicular to the cylinder axis induces surface currents in the $\hat{\boldsymbol{\phi}}$ direction. The corresponding circumferential vector potential has only x- and y-components. Then, because translational invariance guarantees that no physical quantity can depend on the z-coordinate, $E_z = -\partial_z\varphi - \partial_t A_z = 0$. The magnetic field component of interest in this case is B_z, because $E_\phi = cB_z$ in the radiation zone.

A monochromatic plane wave with frequency ω induces time-harmonic currents and thus a time-harmonic scattered field. Outside the cylinder, the electric and magnetic fields satisfy the wave equation. Therefore, the space parts of E_z and B_z satisfy the Helmholtz equation (see Section 16.6),

$$\left[\nabla^2 + \frac{\omega^2}{c^2}\right] u = 0. \tag{21.24}$$

Writing out (21.24) in cylindrical coordinates, we drop the z-derivatives and let $k = \omega/c$ to get

$$\frac{1}{\rho}\frac{\partial}{\partial\rho}\left(\rho\frac{\partial u}{\partial\rho}\right) + \frac{1}{\rho^2}\frac{\partial^2 u}{\partial\phi^2} + k^2 u = 0. \tag{21.25}$$

Separation of variables assumes that $u(\rho, \phi) = R(\rho)G(\phi)$. Inserting this into (21.25) and choosing p^2 as a separation constant gives $G(\phi) = \exp(\pm ip\phi)$ and shows that $R(\rho)$ satisfies Bessel's differential equation with $x = k\rho$:

$$\frac{d^2R}{dx^2} + \frac{1}{x}\frac{dR}{dx} + \left(1 - \frac{p^2}{x^2}\right) R = 0. \tag{21.26}$$

The full angular range of ϕ is relevant, so $p = m$ is a non-negative integer. In Section 7.8.1, we discussed the linearly independent Bessel function solutions $J_m(x)$ and $N_m(x)$. Here, the scattered field must behave like an outgoing cylindrical wave when $\rho \to \infty$. Therefore, the relevant solution is the Hankel function, $H_m^{(1)}(x) = J_m(x) + iN_m(x)$, which has the asymptotic form

$$\lim_{x\to\infty} H_m^{(1)}(x) = \sqrt{\frac{2}{\pi x}}\exp\{i[x - (2m+1)\pi/4]\}. \tag{21.27}$$

We consider $\parallel$ polarization first and write the scattered field, $E_z(\text{scatt})$, as a sum of elementary solutions $H_m^{(1)}(k\rho)\exp(im\phi)$ with expansion coefficients A_m. The incident field is $E_z(\text{inc}) = E_0\exp(ikx)$. Because $x = \rho\cos\phi$ in Figure 21.6, we can use the two-dimensional plane wave expansion (C.52),

$$E_z(\text{inc}) = E_0\exp(ik\rho\cos\phi) = E_0\sum_{m=-\infty}^{\infty} i^m J_m(k\rho)\exp(im\phi), \tag{21.28}$$

and write the total field outside the cylinder as

$$E_z = E_z(\text{inc}) + E_z(\text{scatt}) = E_0\sum_{m=-\infty}^{\infty}\left[i^m J_m(k\rho) + A_m H_m^{(1)}(k\rho)\right]\exp(im\phi). \tag{21.29}$$

The boundary condition $E_z(\rho = a) = 0$ uniquely determines the A_m. Therefore,

$$E_z(\rho, \phi) = E_0 \exp(ik\rho \cos\phi) - E_0 \sum_{m=-\infty}^{\infty} i^m \frac{J_m(ka)}{H_m^{(1)}(ka)} H_m^{(1)}(k\rho) \exp(im\phi). \tag{21.30}$$

The $\perp$ polarization case is similar except that $cB_z(\text{inc}) = E_0 \exp(ikx)$ and the condition that the tangential component of the electric field vanish at the cylinder boundary reads

$$E_\phi(\rho = a) = \frac{c}{k} \frac{\partial B_z}{\partial \rho}\bigg|_{\rho=a} = 0. \tag{21.31}$$

Using a prime to indicate a derivative with respect to the argument, the final result for $\perp$ polarization is

$$cB_z(\rho, \phi) = E_0 \exp(ik\rho \cos\phi) - E_0 \sum_{m=-\infty}^{\infty} i^m \frac{J'_m(ka)}{H_m'^{(1)}(ka)} H_m^{(1)}(k\rho) \exp(im\phi). \tag{21.32}$$

For this two-dimensional problem, the definition of the differential scattering cross section differs slightly from that given earlier. In place of (21.7), we have

$$\frac{d\sigma}{d\phi} = \frac{\rho \hat{\boldsymbol{\rho}} \cdot \langle \mathbf{S}_{\text{rad}} \rangle}{\frac{1}{2} E_0^2 \epsilon_0 c}, \tag{21.33}$$

where the time-averaged Poynting vector in the radiation zone is (cf. Section 20.5.1)

$$\langle \mathbf{S}_{\text{rad}} \rangle_\parallel = \frac{\hat{\boldsymbol{\rho}}}{2} \epsilon_0 c |E_z(\text{rad})|^2 \quad \text{and} \quad \langle \mathbf{S}_{\text{rad}} \rangle_\perp = \frac{\hat{\boldsymbol{\rho}}}{2} \frac{c}{\mu_0} |B_z(\text{rad})|^2. \tag{21.34}$$

The radiation field is the $\rho \to \infty$ part of the scattered field. Therefore, we use the asymptotic formula (21.27) in (21.30) and (21.32), insert the radiation fields into (21.34), and evaluate the cross section expression (21.33) for parallel and perpendicular polarization. The result of these steps is

$$\begin{aligned} \frac{d\sigma_\parallel}{d\phi} &= \frac{2}{\pi k} \left| \sum_{m=-\infty}^{\infty} \frac{J_m(ka)}{H_m^{(1)}(ka)} \exp(im\phi) \right|^2 \\ \frac{d\sigma_\perp}{d\phi} &= \frac{2}{\pi k} \left| \sum_{m=-\infty}^{\infty} \frac{J'_m(ka)}{H_m'^{(1)}(ka)} \exp(im\phi) \right|^2 . \end{aligned} \tag{21.35}$$

These cross sections have dimensions of length (rather than area) because they measure the relative power radiated to infinity per unit length of cylinder, i.e., the power radiated through the boundary of a large circle coaxial with the cylinder.

Integrating each expression in (21.35) over ϕ gives the total scattering cross sections,

$$\sigma_\parallel = \frac{4}{k} \sum_{m=-\infty}^{\infty} \frac{J_m^2(ka)}{J_m^2(ka) + N_m^2(ka)} \qquad \text{and} \qquad \sigma_\perp = \frac{4}{k} \sum_{m=-\infty}^{\infty} \frac{J_m'^2(ka)}{J_m'^2(ka) + N_m'^2(ka)}. \tag{21.36}$$

Figure 21.7 plots $\sigma_\parallel$ and $\sigma_\perp$ as a function of ka. Our first observation is that both cross sections approach a common value when $ka \to \infty$. This is not surprising because geometrical optics becomes valid in the short-wavelength limit. However, instead of approaching the geometricvalue $\sigma_{\text{geom}} = 2a$,

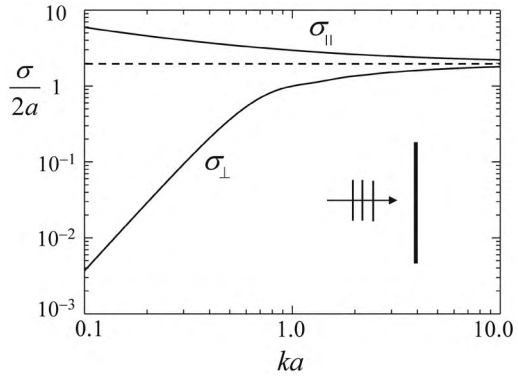

Figure 21.7: The total scattering cross section for plane wave scattering from an infinitely long conducting cylinder (radius a) at normal incidence. $\sigma_{\|}$ and $\sigma_{\perp}$ correspond to **E** parallel and perpendicular to the cylinder axis, respectively. The curves are normalized by the geometric cross section, $\sigma_{\text{geom}} = 2a$.

the limiting value seen in Figure 21.7 is actually *twice* this value. This is called the *extinction paradox* and we will find an explanation for it in Section 21.7.

The low-frequency, long-wavelength behaviors of $\sigma_{\|}$ and $\sigma_{\perp}$ are strikingly different:

$$\lim_{ka\to 0} \sigma_{\|} = \frac{\pi^2}{k \ln^2\left(\dfrac{1}{ka}\right)} \qquad \text{and} \qquad \lim_{ka\to 0} \sigma_{\perp} = \frac{3}{4}\pi^2 a(ka)^3. \tag{21.37}$$

The k^3 behavior of $\sigma_{\perp}$ is the signature of Rayleigh scattering (Section 21.4) in two dimensions. An electric field oriented perpendicular to the cylinder axis drives an electric dipole whose size cannot exceed the diameter of the cylinder. By contrast, no natural length scale limits the surface currents induced along the length of the cylinder when an electric field is oriented parallel to the cylinder axis. That being said, the $1/k$ divergence of $\sigma_{\|}$ in (21.37) is an artifact of the assumed infinite length of the cylinder. For a cylinder with length ℓ, our two-dimensional results apply for observation points (away from the ends) where $a^2/\lambda \ll \rho \ll \ell^2/\lambda$. A reasonable approximation for the cross section in this regime is[6]

$$\sigma_{\|}(\ell) \approx \frac{k\ell^2}{\pi}\sigma_{\|}(\infty). \tag{21.38}$$

Equation (21.38) decreases as ka decreases and crosses over smoothly to three-dimensional Rayleigh scattering when $r \gg \ell^2/\lambda$ and the finite size of the cylinder becomes apparent.

An application of these results is shown in Figure 21.8 where a planar and parallel array of perfectly conducting wires acts as a polarizer for plane electromagnetic waves. When the wire spacing d satisfies $a \ll d \ll \lambda$, waves polarized parallel to the wires are reflected and waves polarized perpendicular to the wires are transmitted. The transmission of $\perp$ waves follows immediately from the vanishingly small interaction between a long-wavelength $\perp$ wave and each wire predicted by Figure 21.7. Long-wavelength $\|$ waves are reflected because, in the limit considered, the longitudinal currents set up in the grid are indistinguishable from the currents set up when a plane wave strikes (and is reflected from) a flat conducting plate.

[6] See Ruck (1970) in Sources, References, and Additional Reading.

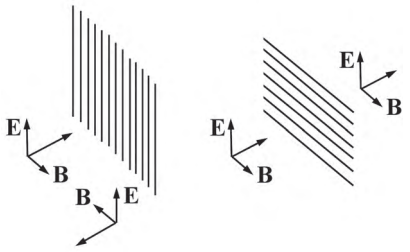

Figure 21.8: A wire-grid polarizer reflects (transmits) waves with **E** parallel (perpendicular) to the direction of the wires in the grid.

21.5.2 Mie Scattering from a Dielectric Sphere

The solution to the electromagnetic problem of plane wave scattering by a dielectric sphere is usually attributed to Gustav Mie.[7] His method was to expand the incident field and the scattered field in an infinite set of vector spherical waves and use the dielectric matching conditions at the surface of the sphere to determine the expansion coefficients. In this section, we outline only the basic steps of this calculation and focus on the results and their interpretation. The key observation is that the incident wave breaks the symmetry of the sphere and makes the matching conditions impossible to satisfy unless the electromagnetic field is written as a linear combination of TE and TM vector spherical waves.

Assume a time dependence $\exp(-i\omega t)$ and put $\omega = ck$. We showed in Section 16.8 that the Maxwell equations have TE and TM vector spherical wave solutions of the form

$$\begin{aligned} \mathbf{E} &= \nabla \times (\mathbf{r}u) - \frac{i}{k}\nabla \times [\nabla \times (\mathbf{r}w)] \\ c\mathbf{B} &= -\nabla \times (\mathbf{r}w) - \frac{i}{k}\nabla \times [\nabla \times (\mathbf{r}u)], \end{aligned} \tag{21.39}$$

where $u(\mathbf{r})$ and $w(\mathbf{r})$ are solutions of the scalar Helmholtz equation,

$$[\nabla^2 + k^2]\psi(\mathbf{r}) = 0. \tag{21.40}$$

We also showed that the separated-variable solutions to (21.40) in spherical coordinates are spherical Bessel radial functions multiplied by spherical harmonic angular functions. However, for the sake of consistency with the majority of the optical, chemical, and atmospheric literature of Mie scattering, we will write sines and cosines for the ϕ dependence and associated Legendre polynomials for the θ dependence [cf. (C.18)].

Beginning with the plane wave identity (C.53), it is an exercise in the use of recurrence relations to show that $\mathbf{E}_{\text{inc}} = E_0 \exp(ikz)\hat{\mathbf{x}}$ can be written in the form (21.39) with

$$\left\{ \begin{array}{c} u_{\text{inc}} \\ w_{\text{inc}} \end{array} \right\} = E_0 \sum_{\ell=1}^{\infty} i^{\ell} \frac{2\ell+1}{\ell(\ell+1)} j_{\ell}(kr) P_{\ell}^{1}(\cos\theta) \left\{ \begin{array}{c} \sin\phi \\ \cos\phi \end{array} \right\}. \tag{21.41}$$

The representation of the scattered field *inside* the sphere also has the form (21.39) with the expansion (21.41) except that $k \to nk$ (where n is the index of refraction of the sphere) and each term in the sum for u_{in} (w_{in}) includes an expansion coefficient c_{ℓ} (d_{ℓ}). The representation of the scattered field *outside* the sphere is again (21.39) with the expansion (21.41) except that the spherical Hankel function $h_{\ell}^{(1)}(kr)$ replaces the spherical Bessel function $j_{\ell}(kr)$ and each term in the sum for u_{out} (w_{out})

[7] Mie published his solution in 1908. An identical solution was published by Ludvig Lorenz in 1890. See the box at the end of the section for more about Lorenz.

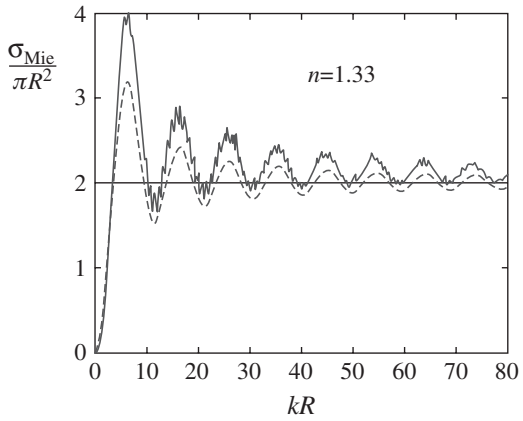

Figure 21.9: The cross section for plane wave scattering from a dielectric sphere with the index of refraction of water: numerical evaluation of exact Mie theory (solid curve); analytic approximation (21.45) (dashed curve). The curves are normalized by the geometric cross section, $\sigma_{\text{geom}} = 4\pi R^2$.

includes an expansion coefficient a_ℓ (b_ℓ). The Hankel function ensures that the exterior field behaves asymptotically like the outgoing spherical wave in (21.3).

The (complex) expansion coefficients a_ℓ, b_ℓ, c_ℓ, and d_ℓ are determined by imposing the four matching conditions at $r = R$:

$$\hat{\mathbf{r}} \times (\mathbf{E}_{\text{inc}} + \mathbf{E}_{\text{out}}) = \hat{\mathbf{r}} \times \mathbf{E}_{\text{in}} \qquad \text{and} \qquad \hat{\mathbf{r}} \times (\mathbf{H}_{\text{inc}} + \mathbf{H}_{\text{out}}) = \hat{\mathbf{r}} \times \mathbf{H}_{\text{in}}. \tag{21.42}$$

The coefficients turn out to be quite complicated, even for non-magnetic spheres. Here, we use a prime to denote differentiation with respect to the argument and display only

$$\begin{aligned} a_\ell &= -\frac{j_\ell(nkR)[xj_\ell(x)]'_{x=kR} - j_\ell(kR)[xj_\ell(x)]'_{x=nkR}}{j_\ell(nkR)[xh_\ell^{(1)}(x)]'_{x=kR} - h_\ell^{(1)}(kR)[xj_\ell(x)]'_{x=nkR}} \\ b_\ell &= -\frac{j_\ell(kR)[xj_\ell(x)]'_{x=nkR} - n^2 j_\ell(nkR)[xj_\ell(x)]'_{x=kR}}{h_\ell^{(1)}(kR)[xj_\ell(x)]'_{x=nkR} - n^2 j_\ell(nkR)[xh_\ell^{(1)}(x)]'_{x=kR}}. \end{aligned} \tag{21.43}$$

The total scattering cross section is

$$\sigma_{\text{Mie}} = \frac{2\pi}{k^2} \sum_{\ell=1}^{\infty} (2\ell + 1) \left\{ |a_\ell|^2 + |b_\ell|^2 \right\}. \tag{21.44}$$

The solid curve in Figure 21.9 is a numerical evaluation of the Mie cross section (21.44) for a sphere with the dielectric constant of water ($n = 1.33$). The dominant features are a sharp rise to a global maximum followed by a quasi-periodic damped oscillation toward an asymptotic value equal to twice the geometric cross section, $\sigma_{\text{geom}} = \pi R^2$. The latter is another of example of the "extinction paradox" mentioned in connection with Figure 21.7. The oscillations come from interfering plane wave rays which accumulate different amounts of phase as they pass through the sphere at different impact parameters. Specifically, if $\Delta = 2R(k_{\text{in}} - k) = 2kR(n - 1)$ is the difference in phase accumulated by a plane wave traversing the sphere diameter and a plane wave propagating in vacuum, the dashed curve in Figure 21.9 is the prediction of an approximate cross section formula we will derive in Application 21.2 of Section 21.7.1:

$$\sigma_{\text{approx}} = 2\pi R^2 \left[1 - \frac{2}{\Delta} \sin \Delta + \frac{2}{\Delta^2} (1 - \cos \Delta) \right]. \tag{21.45}$$

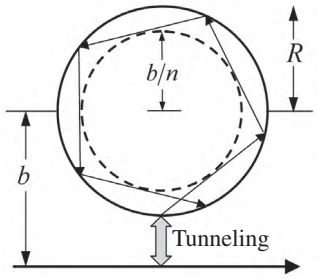

Figure 21.10: Ray-optic representation of the coupling between an incident wave and a normal mode of a spherical dielectric resonator. The radial boundaries are the inner and outer turning points of the effective potential in Figure 19.24 at the energy of the mode. Figure after Guimarães and Nussenzveig (1992). Copyright 1992, with permission from Elsevier.

The high-frequency, non-periodic "ripples" which decorate the damped oscillation in Figure 21.9 persist out to arbitrarily large values of kR and are extraordinarily sensitive to changes in the index n and the sphere radius R. Each ripple is a resonance in the cross section which occurs when the incident wave transiently couples to one of the electromagnetic normal modes of the dielectric sphere. To understand this, we recall from Section 19.7 that these modes can be described as virtual bound states trapped by the centrifugal barrier of the ℓ-dependent effective potential sketched in Figure 19.24. By analogy with the quantum theory of potential scattering, we identify $\ell = bk$ as the angular momentum of a ray with impact parameter b. If $b < R$, the ray simply refracts into the sphere in the usual way. If $b \gg R$, there is virtually no interaction between the ray and the sphere. In between, there is a range of impact parameters where the ray can tunnel through the barrier and resonantly excite a normal mode.[8] Figure 21.10 represents the mode by a ray which propagates inside the sphere in the annular volume defined by the inner turning point of the potential at $r = b/n$ and the outer turning point at $r = R$. Eventually, the ray tunnels back out and rejoins the original ray.

The Great Dane

Eighteen years before Gustav Mie published his analysis of what we call "Mie" scattering, the entire problem was solved and published by the Danish physicist Ludvig Lorenz (1829-1891). Remarkably, this is only one of several instances where Lorenz' precedence in the solution of an electromagnetic problem went unrecognized by his peers and forgotten by history. For most of the last century, he was remembered only for the Lorentz-Lorenz equation, which generalizes the Clausius-Mossotti relation of static dielectric theory and relates the index of refraction $n(\omega)$ of a gas of molecules with density N to the molecular polarizability, $\alpha(\omega)$:

$$\frac{n^2(\omega) - 1}{n^2(\omega) + 2} = \frac{N\alpha(\omega)}{3\epsilon_0}.$$

The pairing of Lorenz with the Dutch physicist Hendrik Lorentz is particulary ironic because the familiar electromagnetic gauge choice,

$$\nabla \cdot \mathbf{A} + \frac{1}{c^2}\frac{\partial \varphi}{\partial t} = 0,$$

has long been incorrectly attributed to Lorentz. In fact, this gauge constraint first appeared in 1867 when Lorenz introduced the concept of the retarded potential into electrodynamics in a paper

[8] The "tunneling" wave is an evanescent wave of the sort discussed in Section 17.3.7.

entitled "On the identity of the vibrations of light with electrical currents". Lorenz generalized a quasistatic theory of Kirchhoff to include retardation and developed a theory which (in retrospect) was practically identical to Maxwell's. Lorenz went to some trouble to insist that the concept of the aether was superfluous.

A third example of neglect dates from 1860, when Lorenz extended Fresnel's theory of refraction to account for a thin "transition layer" between two bulk media where the dielectric properties interpolate smoothly between the two bulk values. The elliptical polarization of the reflected light induced by the presence of this layer became the diagnostic tool of "ellipsometry" 40 years later when Drude re-derived Lorenz' results using Maxwell theory.

It is puzzling that Lorenz' work was forgotten so quickly. His most important papers were quickly translated from Danish and all of his work could be read in German, French, or English by 1896, when his collected Works were published. On the other hand, Lorenz was an autodidact who did not correspond much with other physicists. He did not travel widely and spent his entire career as a physics teacher for army cadets at a military high school outside Copenhagen. For a man born in the Danish city of Elsinore (the setting for Shakespeare's *Hamlet*), it would be altogether fitting if the ghost of his achievements walked again among contemporary scientists.

21.6 Two Approximation Schemes

Modern computers can generate essentially exact solutions to most electromagnetic scattering problems. Nevertheless, one always gains intuition from less exact methods if they are based on physically well-motivated approximations. This section treats two such schemes. The *Born approximation* applies to objects which are only weakly polarizable, magnetizable, or conducting, but where the ratio of the object size to the wavelength (a/λ) can have any value. The *physical optics approximation* applies to highly conducting objects in the limit when $a/\lambda \gg 1$.

21.6.1 The Born Approximation

The Born approximation presumes that the total field $\mathbf{E}$ inside a weakly dielectric or weakly conducting scattering medium does not differ significantly from the incident field $\mathbf{E}_{\text{inc}}$. If we use the language of polarization (rather than conductivity), this means that the current induced in the object by a monochromatic plane wave is

$$\mathbf{j} = \frac{\partial \mathbf{P}}{\partial t} = -i\omega\epsilon_0\chi_e\mathbf{E} \approx -i\omega\epsilon_0\chi_e\mathbf{E}_{\text{inc}} = -i\omega\epsilon_0\chi_e\hat{\mathbf{e}}_0 E_0 \exp[(i\mathbf{k}_0\cdot\mathbf{r} - \omega t)]. \tag{21.46}$$

Substituting (21.46) into (21.7) gives the approximate cross section

$$\left.\frac{d\sigma_{\text{scatt}}}{d\Omega}\right|_{\text{Born}} = \left(\frac{k_0^2}{4\pi}\right)^2 |\hat{\mathbf{k}}\times\hat{\mathbf{e}}_0|^2 \left|\int d^3r'\,\chi_e(\mathbf{r},\omega)\exp[i(\mathbf{k}_0-\mathbf{k})\cdot\mathbf{r}']\right|^2. \tag{21.47}$$

The angular factor $|\hat{\mathbf{k}}\times\hat{\mathbf{e}}_0|^2$ in (21.47) is familiar from (21.11) and all the remarks made there about averaging this quantity for an unpolarized incident wave apply here also.

A low-frequency application of (21.47) applies to a dielectric object with volume V and uniform electric susceptibility χ_e. When $k_0 a \ll 1$, the exponential may be neglected in the integral and (21.47) reduces to

$$\left.\frac{d\sigma_{\text{scatt}}}{d\Omega}\right|_{\text{Born}} = \left(\frac{k_0^2}{4\pi}\right)^2 (V\chi_e)^2 |\hat{\mathbf{k}}\times\hat{\mathbf{e}}_0|^2. \tag{21.48}$$

The polarizability of this object is $\alpha = \epsilon_0 V \chi_e$. Therefore, (21.48) reproduces the Rayleigh scattering formula (21.22), as expected.

A high-frequency application of (21.47) applies to a Drude plasma where (see Section 18.5.1)

$$\chi_e(\omega) = \frac{\epsilon(\omega)}{\epsilon_0} - 1 = \left(1 - \frac{\omega_p^2}{\omega^2}\right) - 1 = -\frac{nq^2}{\omega^2 m \epsilon_0}. \tag{21.49}$$

Generalizing to a particle density $n(\mathbf{r})$ which varies with position, substituting (21.49) into (21.47) gives

$$\left.\frac{d\sigma_{\text{scatt}}}{d\Omega}\right|_{\text{Born}} = \left(\frac{q^2}{4\pi\epsilon_0 mc^2}\right)^2 |\hat{\mathbf{k}} \times \hat{\mathbf{e}}_0|^2 \left| \int d^3r' \, n(\mathbf{r}') \exp[i(\mathbf{k}_0 - \mathbf{k}) \cdot \mathbf{r}'] \right|^2. \tag{21.50}$$

If the mobile particles of the plasma are electrons, where $q = -e$, (21.50) reproduces the Thomson scattering results of Section 21.3 multiplied by a form factor which reproduces the results of Example 21.2.

Example 21.3 Find the Born approximation to the differential cross section for scattering from a uniform and lossless dielectric sphere with radius R. Plot the cross section for an unpolarized incident beam with $k_0 R = 15/2$.

Solution: The susceptibility χ_e is constant inside the sphere and zero outside the sphere. We make no assumptions about the magnitude of $k_0 R$. With $\mathbf{q} = \mathbf{k} - \mathbf{k}_0$, (21.47) becomes

$$\left.\frac{d\sigma_{\text{scatt}}}{d\Omega}\right|_{\text{Born}} = \left(\frac{k_0^2 \chi_e}{4\pi}\right)^2 |\hat{\mathbf{k}} \times \hat{\mathbf{e}}_0|^2 \left| \int d^3r' \, \exp(i\mathbf{q} \cdot \mathbf{r}') \right|^2.$$

The integral to be evaluated is

$$I = \int d^3r' \, \exp(i\mathbf{q} \cdot \mathbf{r}') = 2\pi \int_{-1}^{1} du \int_0^R dr' r'^2 \exp(iqru) = \frac{4\pi}{q} \int_0^R dr' r' \sin(qr') = 4\pi R^3 \frac{j_1(qR)}{qR},$$

where $j_1(x) = \sin(x)/x^2 - \cos(x)/x$ is the spherical Bessel function of order one. The scattering is elastic, so the remark at the end of Example 21.2 tells us that $q = 2k_0 \sin(\theta/2)$. Finally, (21.20) shows that $|\hat{\mathbf{k}} \times \hat{\mathbf{e}}_0|^2 = \frac{1}{2}(1 + \cos^2\theta)$ for an unpolarized incident wave. We conclude that the Born cross section for the sphere is

$$\left.\frac{d\sigma_{\text{scatt}}}{d\Omega}\right|_{\text{Born}} = \frac{R^2}{4}(k_0 R)^2 \chi_e^2 \frac{1 + \cos^2\theta}{2} \frac{j_1^2[2k_0 R \sin(\theta/2)]}{\sin^2(\theta/2)}.$$

Figure 21.11 compares the Born approximation (solid line) to the differential scattering cross section with the exact Mie cross section (dashed curve) for a dielectric sphere with index of refraction $n = 1.05$ and radius $R = (15/4\pi)\lambda$. The majority of the scattering is near the forward direction, as one might expect from a sphere whose dielectric properties are so weak that the field inside the sphere is indistinguishable from the incident field. The zeroes of the Born cross section (which come from the zeroes of the spherical Bessel function) are replaced by local minima in

the Mie cross section. Physically, the zeroes (minima) come from wave interferences of the sort discussed in Section 21.5.2.

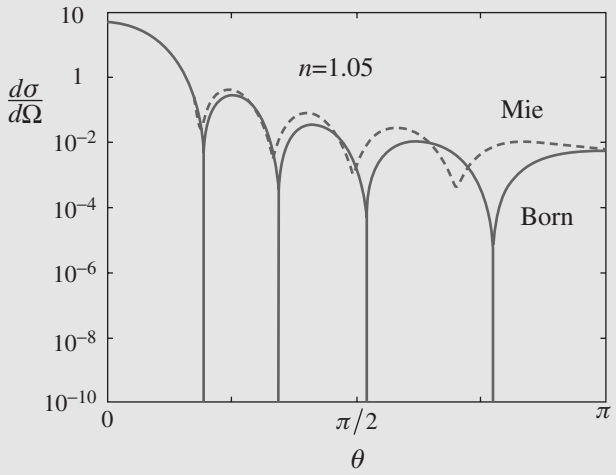

Figure 21.11: Differential cross section (in arbitrary units) for scattering from a uniform dielectric sphere with index of refraction $n = 1.05$ and radius $R = (15/4\pi)\lambda$. The exact Mie result is the dashed curve. The Born approximation is the solid curve.

21.6.2 The Physical Optics Approximation

Geometrical optics is the natural starting point for scattering situations where the wavelength of the incident wave is very small compared to the characteristic feature size of a target object. Such objects are called *electrically large*. For a plane wave incident on a conductor, the frequency-independent physics of geometrical optics is simply specular reflection of a parallel set of rays from the illuminated portions of the target object. The points on the surface shadowed from the incident wave by other parts of the body play no role.

The physical optics approximation is a physically motivated correction to geometrical optics which simplifies the radiation fields computed from Maxwell's equations. The key idea, due to Macdonald (1912), is to assign a current density $\mathbf{K}$ to every illuminated surface point as if that point were part of a flat and infinite conducting plane oriented tangent to the surface at that point. Zero surface current density is assigned to surface points which are shadowed. From Section 19.3.1, we know that specular reflection of a plane wave incident on a conducting plane annuls the tangential component of the surface electric field and doubles the tangential component of the surface magnetic field. Hence, the physical optics approximation for the current density induced on the surface of a conducting object by the incident wave is

$$\mu_0 \mathbf{K}(\mathbf{r}, t) = \begin{cases} 2\hat{\mathbf{n}} \times \mathbf{B}_{\text{inc}}(\mathbf{r}, t) & \text{at illuminated surface points,} \\ 0 & \text{at shadowed surface points.} \end{cases} \tag{21.51}$$

If S is the illuminated part of the surface and $\mathbf{B}_{\text{inc}} = \mathbf{B}_0 \exp[i(\mathbf{k}_0 \cdot \mathbf{r} - \omega t)]$ is the magnetic field of the incident plane wave, substituting (21.51) into the vector potential expression (20.118) to evaluate

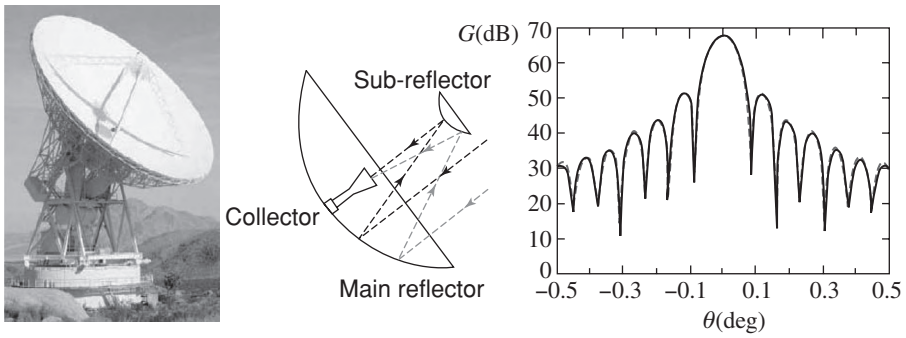

Figure 21.12: Left panel: a parabolic reflector antenna. Middle panel: geometrical optics ray tracing of an incoming bundle of parallel rays. Right panel: physical optics prediction for the gain, $G(\theta)$, which is the angular distribution of power received by this reflector, normalized by the total power received. The vertical scale (decibels) is logarithmic. Figure adapted from Imbriale (2003).

the electric field in (20.119) gives

$$\mathbf{E}_{\rm rad}(\mathbf{r},t) \approx \frac{i\omega}{2\pi}\frac{\exp[i(kr-\omega t)]}{r}\hat{\mathbf{k}}\times\left\{\hat{\mathbf{k}}\times\int_S dS'\,(\hat{\mathbf{n}}'\times\mathbf{B}_0)\exp[i(\mathbf{k}_0-\mathbf{k})\cdot\mathbf{r}']\right\}. \tag{21.52}$$

A common use of (21.52) is to calculate the angular distribution of radiation transmitted or received (they are the same) by an electrically large antenna.[9] For example, the reflector-type radio antenna shown in the leftmost panel of Figure 21.12 is part of the NASA Deep Space Network. The middle panel of the figure shows the geometrical optics prediction that parallel rays received from space are focused by the main parabolic reflector onto a sub-reflector which reflects them onto a collector. The rightmost panel shows the physical optics prediction for the gain function (the angular distribution normalized by the total power) at 7.2 GHz for the particular 32 m diameter antenna shown in the leftmost panel. The polar angle θ is measured with respect to the symmetry axis of the main reflector paraboloid. Because the vertical scale (decibels) is logarithmic, the physical optics gain function confirms the geometrical optics expectation that most of the received power is confined to a very small angular range around the symmetry axis. Discussion of the side lobes in $G(\theta)$ is best postponed until Section 21.8 when we take up the subject of diffraction.

21.7 The Total Cross Section

We have so far neglected the possibility that the scatterer in Figure 21.2 could *absorb* some of the energy carried by the incident monochromatic plane wave. To account for this, we invoke conservation of energy and evaluate the Poynting theorem for a volume V which includes the scatterer:

$$\int_V d^3r\,\nabla\cdot\mathbf{S}+\frac{d}{dt}U_{\rm EM}=-\int_V d^3r\,\mathbf{j}\cdot\mathbf{E}. \tag{21.53}$$

[9] See the footnote which accompanies (20.124).

The total energy term in (21.53) drops out after averaging over one period of a time-harmonic field. Therefore,

$$\int_S dA\,\hat{\mathbf{n}}\cdot\langle\mathbf{S}\rangle = -\int_V d^3r\,\langle\mathbf{j}\cdot\mathbf{E}\rangle. \tag{21.54}$$

The right side of (21.54) is the rate at which field energy is absorbed by the particles of the scatterer. This motivates us to define the total cross section for absorption, $\sigma_{\rm abs}$, as the ratio of the time-averaged absorption rate to the time-averaged rate at which the incident beam supplies energy per unit area:

$$\sigma_{\rm abs} = \frac{1}{|\langle\mathbf{S}_{\rm inc}\rangle|}\int_V d^3r\,\langle\mathbf{j}\cdot\mathbf{E}\rangle = -\frac{1}{|\langle\mathbf{S}_{\rm inc}\rangle|}\int_S dA\,\hat{\mathbf{n}}\cdot\langle\mathbf{S}\rangle. \tag{21.55}$$

The total cross section is the sum of the cross sections for scattering and absorption:

$$\sigma_{\rm tot} = \sigma_{\rm scatt} + \sigma_{\rm abs}. \tag{21.56}$$

21.7.1 The Optical Theorem

The *optical theorem* is an exact relation which relates the total cross section (21.56) to the amplitude of the electromagnetic field scattered in the forward direction (the propagation direction of the incident wave). To derive it, we choose the closed integration surface S in (21.55) as a sphere (centered on the scatterer) whose surface lies entirely in the radiation zone. Then, because the flux of the incident plane wave in (21.3) is $|\langle\mathbf{S}_{\rm inc}\rangle| = \frac{1}{2}\epsilon_0 c E_0^2$, we can rewrite the leftmost and rightmost members of (21.55) as

$$-\sigma_{\rm abs} = \frac{1}{E_0^2}{\rm Re}\int d\Omega\, r^2\hat{\mathbf{r}}\cdot\left[(\mathbf{E}_{\rm inc}+\mathbf{E}_{\rm rad})^*\times c(\mathbf{B}_{\rm inc}+\mathbf{B}_{\rm rad})\right]. \tag{21.57}$$

The integral in (21.57) which involves $\mathbf{E}^*_{\rm inc}\times\mathbf{B}_{\rm inc}$ is zero because $\mathbf{S}_{\rm inc}$ is uniform in space. From (21.4), the integral which involves $\mathbf{E}^*_{\rm rad}\times\mathbf{B}_{\rm rad}$ is $\sigma_{\rm scatt}$. The cross terms which remain can be evaluated using (21.3) and $c\mathbf{B} = \hat{\mathbf{k}}_0\times\mathbf{E}_{\rm inc} + \hat{\mathbf{r}}\times\mathbf{E}_{\rm rad}$.

Because $\hat{\mathbf{r}}\cdot\mathbf{f} = 0$, the remarks just above render (21.57) in the form

$$\begin{aligned}-\sigma_{\rm abs} = \sigma_{\rm scatt} &+ {\rm Re}\int d\Omega\,(\hat{\mathbf{e}}_0^*\cdot\mathbf{f})\exp(-i\mathbf{k}_0\cdot\mathbf{r})\,r\exp(ikr)\\ &+ {\rm Re}\int d\Omega\left[(\hat{\mathbf{r}}\cdot\hat{\mathbf{k}}_0)(\hat{\mathbf{e}}_0\cdot\mathbf{f}^*) - (\hat{\mathbf{r}}\cdot\hat{\mathbf{e}}_0)(\hat{\mathbf{k}}_0\cdot\mathbf{f}^*)\right]\exp(i\mathbf{k}_0\cdot\mathbf{r})\,r\exp(-ikr).\end{aligned} \tag{21.58}$$

We evaluate the integrals in (21.58) using the asymptotic identity:

$$\lim_{k_0r\to\infty}\exp(i\mathbf{k}_0\cdot\mathbf{r}) = 2\pi i\left[\frac{\exp(-ik_0r)}{k_0r}\delta(\hat{\mathbf{r}}+\hat{\mathbf{k}}_0) - \frac{\exp(ik_0r)}{k_0r}\delta(\hat{\mathbf{r}}-\hat{\mathbf{k}}_0)\right]. \tag{21.59}$$

The reader can derive (21.59) by substituting the spherical harmonic addition theorem (C.23) into the plane wave expansion formula (C.53) to get

$$\exp(i\mathbf{k}_0\cdot\mathbf{r}) = 4\pi\sum_{\ell=0}^{\infty} i^\ell j_\ell(k_0r)\sum_{m=-\ell}^{\ell} Y^*_{\ell m}(\hat{\mathbf{k}}_0)Y_{\ell m}(\hat{\mathbf{r}}). \tag{21.60}$$

After inserting the large-argument form of the spherical Bessel function (C.46) into (21.60), the inversion symmetry (C.24) and completeness (C.20) of the spherical harmonics produces (21.59).

Substituting (21.59) into (21.58) eliminates one integral because the factor $\hat{\mathbf{r}}\cdot\hat{\mathbf{e}}_0$ vanishes when $\hat{\mathbf{r}} = \pm\hat{\mathbf{k}}_0$. Otherwise, we note that $\hat{\mathbf{r}} = \hat{\mathbf{k}}_0$ is the $\theta = 0$ forward direction and $\hat{\mathbf{r}} = -\hat{\mathbf{k}}_0$ is the $\theta = \pi$

backward direction. Therefore, because $k = k_0$, the remaining integrals and (21.56) reduce (21.58) to

$$-\sigma_{\text{tot}} = -\frac{4\pi}{k}\text{Re}\left[\frac{\hat{\mathbf{e}}_0^* \cdot \mathbf{f}(\mathbf{k}_0) - \hat{\mathbf{e}}_0 \cdot \mathbf{f}^*(\mathbf{k_0})}{2i} - \frac{\hat{\mathbf{e}}_0^* \cdot \mathbf{f}(-\mathbf{k}_0)e^{i2kr} + \hat{\mathbf{e}}_0 \cdot \mathbf{f}^*(-\mathbf{k}_0)e^{-i2kr}}{2i}\right]. \quad (21.61)$$

The first (second) term in square brackets in (21.61) is purely real (imaginary). Therefore, (21.61) reduces to our desired result, the optical (or forward scattering) theorem:

$$\sigma_{\text{tot}} = \frac{4\pi}{k}\text{Im}\left[\hat{\mathbf{e}}_0^* \cdot \mathbf{f}(\mathbf{k}_0)\right]. \quad (21.62)$$

Because (21.62) was derived from (21.55), conservation of energy is the physical principle which underlies the optical theorem. The flow of energy is determined by the interference between the incident wave and the wave created by the excitation of the scatterer. This interference happens at all points in space, but only the amplitude of the radiated wave in the forward direction appears in the final statement of the theorem.

Two points are worth noting. First, our proof of (21.62) assumed an incident (plane) wave with infinite extent in the transverse direction. The theorem does not apply to a beam-like wave if its transverse width is smaller than the size of the scatterer. Second, the theorem is exact and therefore easy to violate when approximate expressions are used for σ_{tot} or $\mathbf{f}(\mathbf{k}_0)$. An example is the Thomson scattering calculation performed in Section 21.3. We found $\sigma_{\text{scatt}} = (8\pi/3)r_e^2$, yet $\hat{\mathbf{e}}_0^* \cdot \mathbf{f}(\mathbf{k}_0)$ was purely real. This is not consistent with (21.62).

To identify the problem, we use (21.55) and (21.56) and write the theorem in the form

$$\frac{4\pi}{k}\text{Im}\left[\hat{\mathbf{e}}_0^* \cdot \mathbf{f}(\mathbf{k}_0)\right] = \sigma_{\text{scatt}} + \frac{1}{2|\langle \mathbf{S}_{\text{inc}} \rangle|}\text{Re}\left[\int d^3r\, \mathbf{j}^* \cdot \mathbf{E}_{\text{inc}} + \int d^3r\, \mathbf{j}^* \cdot \mathbf{E}_{\text{rad}}\right]. \quad (21.63)$$

Equation (21.63) splits σ_{abs} into two terms. For Thomson scattering, the contribution $\int d^3r\, \mathbf{j}^* \cdot \mathbf{E}_{\text{inc}} = 0$ because a single electron has no internal dynamics to dissipate energy. On the other hand, $\int d^3r\, \mathbf{j}^* \cdot \mathbf{E}_{\text{rad}} \neq 0$ because the radiation field does work on the electron. This is the phenomenon of *radiation reaction*, which we neglected when writing the equation of motion (21.9) but which contributes an imaginary part to $\mathbf{f}(\mathbf{k}_0)$ when it is taken into account.[10] This omission is justified as far as the particle dynamics is concerned. It is *not* justified when we study conservation of energy as reflected in the optical theorem.

Application 21.2 Approximate Mie Scattering

This Application uses the optical theorem to derive the approximate cross section formula (21.45) for wave scattering from a sphere with index of refraction n. The idea is to replace the asymptotic electric field (21.3) by a scalar wave with the same form and mimic the partial-wave expansion of the scattering amplitude $f(\theta)$ which appears, e.g., in the quantum theory of potential scattering. This expansion uses a set of phase shifts, δ_ℓ, to parameterize the scattering:

$$f(\theta) = \frac{1}{2ik}\sum_{\ell=0}^{\infty}(2\ell+1)P_\ell(\cos\theta)\left[\exp(i2\delta_\ell) - 1\right]. \quad (21.64)$$

Following the ray optics discussion at the end of Section 21.5.2, we use $\ell = bk$ to replace the angular momentum index in (21.64) by the impact parameter $b = R\cos\alpha$ shown in Figure 21.13. A straight-line ray with this impact parameter accumulates a phase shift $2\delta_\ell = \Delta\sin\alpha$ with respect to a wave in vacuum where $\Delta = 2R(k_{\text{in}} - k_{\text{out}}) = 2kR(n-1)$.

[10] See Section 23.6.

We evaluate (21.64) in a continuum approximation where

$$\sum_{\ell=0}^{\infty} \to k \int_0^R db = kR \int_0^{\pi/2} d\alpha \sin\alpha. \tag{21.65}$$

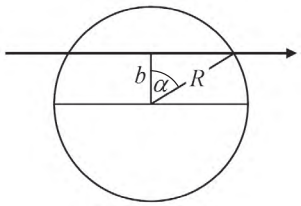

Figure 21.13: A ray passes through a dielectric sphere with impact parameter b.

Therefore, because $P_\ell(1) = 1$ and $2\ell + 1 \approx 2kR\cos\alpha$, the forward scattering amplitude becomes

$$f(0) = -ikR^2 \int_0^{\pi/2} d\alpha \sin\alpha\cos\alpha \left[\exp(i\Delta\sin\alpha) - 1\right]. \tag{21.66}$$

The substitution $x = \sin\alpha$ and an integration by parts yields

$$f(0) = ikR^2 \left[\frac{1}{2} - \frac{\exp(i\Delta)}{i\Delta} - \frac{\exp(i\Delta) - 1}{\Delta^2}\right]. \tag{21.67}$$

Replacing $\hat{\mathbf{e}}_0^* \cdot \mathbf{f}$ by f in the optical theorem (21.62) gives the cross section (21.45):

$$\sigma_{\text{approx}} = 2\pi R^2 \left[1 - \frac{2}{\Delta}\sin\Delta + \frac{2}{\Delta^2}(1 - \cos\Delta)\right]. \tag{21.68}$$

■

21.7.2 The Extinction Paradox

Consider an object of linear size a which does not absorb energy. In the short-wavelength limit when $ka \gg 1$, our experience with optics suggests that $\sigma_{\text{tot}} = \sigma_{\text{scatt}}$ will approach the geometric cross section σ_{geom}.[11] However, both Figure 21.7 for a conducting cylinder and Figure 21.9 for a dielectric sphere show, instead, that σ_{scatt} approaches *twice* this value. These are examples of a more general high-frequency result, called the *extinction paradox*, which is valid even when $\sigma_{\text{abs}} \neq 0$, namely, $\sigma_{\text{tot}} \to 2\sigma_{\text{geom}}$ when $ka \gg 1$.

We resolve this paradox (at least qualitatively) by paying careful attention to the scattered field in (21.1). The key is the Ewald-Oseen extinction theorem (see Section 20.9.1), which can be interpreted as dividing $\mathbf{E}_{\text{scatt}}$ into three parts. The first part annihilates the incident wave inside the object; the second part forms the entire wave field inside the object; the final part superposes with the incident field to form the entire wave field outside the object. With these in mind, we consider two objects: one perfectly conducting and one perfectly absorbing. In both cases, the short-wavelength limit $ka \gg 1$ implies that a dark and sharply defined shadow forms behind the object.

For the perfect conductor, $\sigma_{\text{abs}} = 0$ and the entire effect comes from σ_{scatt}. One contribution to σ_{scatt} comes from the incident wave power which is reflected from the illuminated face of the object. By definition, this piece has magnitude σ_{geom}. Another contribution comes from the power in the

[11] See the last line of Section 21.2 for the definition of σ_{geom}.

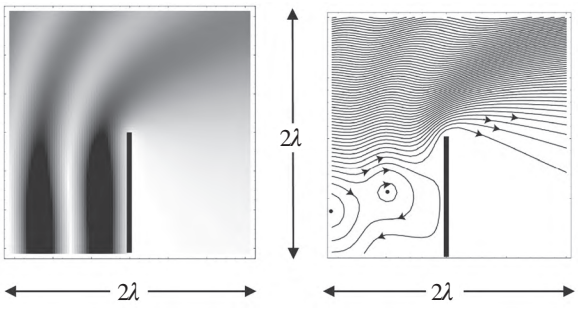

Figure 21.14: A plane wave incident from the left diffracts at the edge of a conducting half-plane (vertical black line). The electric field points out of the plane of the diagram. Left panel: electric field intensity; right panel: lines of the Poynting vector. Both panels are two wavelengths on a side. Figure from Berry (2001).

scattered wave which forms the shadow. This also has magnitude $\sigma_{\rm geom}$ because complete destructive interference requires that $\mathbf{E}_{\rm scatt} = -\mathbf{E}_{\rm inc}$ in the shadow region. The final result is $\sigma_{\rm scatt} = 2\sigma_{\rm geom}$. For the perfect absorber, $\sigma_{\rm abs} = \sigma_{\rm geom}$ because the field created inside the object now contains all the power which was reflected in the previous case. On the other hand, $\sigma_{\rm scatt} = \sigma_{\rm geom}$ because the formation of the shadow still requires that the sources inside the sphere annihilate the incident field in the shadow region. This gives $\sigma_{\rm tot} = 2\sigma_{\rm geom}$ as a consequence of (21.56).

So far, we have relied on the presence of a sharp shadow (and thus the large-object limit $ka \gg 1$) to explain the extinction paradox. However, numerical studies by Berg *et al.* (2011) show that $\sigma_{\rm tot} \to 2\sigma_{\rm geom}$ even for scattering from semi-transparent dielectric spheres where no shadow forms because ka is *not* large. If we generalize the definition of Δ in Application 21.2 to

$$\Delta = 2ka\,{\rm Re}(n-1), \tag{21.69}$$

a summary of the numerical results for a sphere is

$$\lim_{\Delta \gg 1} \sigma_{\rm tot} = 2\sigma_{\rm geom}. \tag{21.70}$$

Some insight into (21.70) comes from studying the integration over angles of $d\sigma_{\rm tot}/d\Omega$ for spheres with a complex index of refraction. When this integration is carried out over the illuminated part of the sphere's surface *alone*, the result is very nearly $2\sigma_{\rm geom}$ for all values of Δ. Continuing the integration over the non-illuminated part of the surface drives the integral away from this value *except* when $\Delta \gg 1$. In that case, $\sigma_{\rm tot}$ remains equal to $2\sigma_{\rm geom}$ because either (i) the contributions from every part of the non-illuminated surface are negligibly small (the shadow-forming conductor case) or (ii) the contributions from different parts of the non-illuminated surface vary rapidly in phase and cancel one another out (the non-shadow-forming dielectric case). It remains an open question to prove (21.70) rigorously for an arbitrary scatterer.

21.8 Diffraction by a Planar Aperture

Wave scattering from an object with a sharp edge is called *diffraction*. The first solution of the Maxwell equations for a true diffraction problem appeared in 1896, when Sommerfeld published his *tour de force* analysis of a plane wave incident on a semi-infinite conducting plane. Figure 21.14 illustrates some features of Sommerfeld's solution. The vertical dark line at the center of the each panel is the half-plane, which extends infinitely in three directions: downward, toward the reader, and away from the reader. The plane wave propagates from left to right with the electric vector $\mathbf{E}$ oriented perpendicular to the page. The shading in the left panel is darkest (lightest) in regions of highest

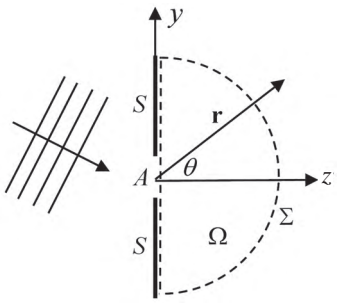

Figure 21.15: A monochromatic plane wave incident on an aperture (A) cut out of a plane screen (S). The dashed curve Σ is the surface of the volume Ω.

(lowest) electric field strength. The appearance of non-zero field intensity in the geometric shadow of the screen is one of the characteristic signatures of diffraction by a sharp edge.

The right panel of Figure 21.14 shows streamlines of the Poynting vector $\mathbf{S} = \mathbf{E} \times \mathbf{H}$ during edge diffraction. Several of these paths for energy flow bend around the edge and into the geometrical shadow. Other lines of $\mathbf{S}$ illustrate the reflection of the incident wave from the conducting surface. The small closed circle on the illuminated side of the plane is centered at one of many isolated points (actually lines perpendicular to the page) where the electric field vanishes. This may be compared to the parallel lines (or planes perpendicular to the page) of zero electric field which occur in the standing wave which forms when a plane wave falls with normal incidence on an infinite (rather than semi-infinite) conducting plane (see Section 19.3.1).

Broadly viewed, edge diffraction by a semi-infinite plane is a special case of electromagnetic diffraction from an aperture cut out of a flat screen. This more general problem—with screens made from different materials and single or multiple apertures shaped like circles, rectangles, or long narrow slits—has long attracted the attention of physicists, microscopists, and astronomers. We follow tradition and analyze this situation first using scalar diffraction theory. We then solve the problem in a manner that is fully consistent with the Maxwell equations.

21.8.1 Scalar Diffraction Theory

Figure 21.15 shows a monochromatic plane wave incident on an aperture (A) cut out of a planar screen (S) at $z = 0$. Scalar diffraction theory treats the plane wave as a scalar field and seeks the unique solution to the wave equation which propagates into the $z > 0$ half-space subject to suitable boundary conditions on the screen and at infinity. The guess $u(\mathbf{r}) \exp(-i\omega t)$ implies that $u(\mathbf{r})$ satisfies Helmholtz' equation (21.24), and the Green function method is particularly well suited to our task. If $k_0 = \omega/c$, the Green function of interest satisfies

$$\left[\nabla^2 + k_0^2\right] G(\mathbf{r}, \mathbf{r}') = -\delta(\mathbf{r} - \mathbf{r}'). \tag{21.71}$$

The key step uses $u(\mathbf{r})$ and $G(\mathbf{r}', \mathbf{r})$ to write out Green's second identity (1.80) for the volume Ω enclosed by the surface Σ indicated in Figure 21.15. Ω comprises the entire $z > 0$ half-plane when we let the radius of the hemisphere go to infinity.

The identity in question reads

$$\int_\Omega d^3r' \left[u(\mathbf{r}')\nabla'^2 G(\mathbf{r}', \mathbf{r}) - G(\mathbf{r}', \mathbf{r})\nabla'^2 u(\mathbf{r}')\right] = \int_\Sigma d\mathbf{S}' \cdot \left[u(\mathbf{r}')\nabla' G(\mathbf{r}', \mathbf{r}) - G(\mathbf{r}', \mathbf{r})\nabla' u(\mathbf{r}')\right]. \tag{21.72}$$

For $\mathbf{r} \in \Omega$, (21.24) and (21.71) reduce (21.72) to

$$u(\mathbf{r}) = \int_{\Sigma} d\mathbf{S}' \cdot \left[G(\mathbf{r}', \mathbf{r}) \nabla' u(\mathbf{r}') - u(\mathbf{r}') \nabla' G(\mathbf{r}', \mathbf{r}) \right]. \tag{21.73}$$

Our previous experience with Green functions suggests that we impose boundary conditions on (21.71) so one of the two terms in (21.73) vanishes. We choose a Dirichlet condition on the planar surface $z = 0^+$ and an outgoing spherical wave condition at infinity:

$$G(\mathbf{r}', \mathbf{r}) = 0 \quad \text{when} \quad z' = 0^+$$

and

$$r' \left(\frac{\partial G}{\partial r'} - ik_0 G \right) = 0 \quad \text{when} \quad r' \to \infty. \tag{21.74}$$

The second of these guarantees that the integral over the large hemispherical part of Σ vanishes. Therefore, because the outward normal to Ω along the screen is $-\hat{\mathbf{z}}$, (21.73) simplifies to

$$u(\mathbf{r}) = \int_{z'=0^+} dS' u(\mathbf{r}') \frac{\partial}{\partial z'} G(\mathbf{r}', \mathbf{r}). \tag{21.75}$$

We now need an explicit expression for $G(\mathbf{r}', \mathbf{r})$. A good starting point is the free-space Green function (20.53), which satisfies both (21.71) and the outgoing wave condition (see Section 20.3.3):

$$G_0(\mathbf{r}, \mathbf{r}') = \frac{\exp\left(ik_0 |\mathbf{r} - \mathbf{r}'|\right)}{4\pi |\mathbf{r} - \mathbf{r}'|}. \tag{21.76}$$

Using (21.76) and the method of images (Section 8.3), it is straightforward to construct a Green function which vanishes when $z' = 0^+$, in accordance with (21.8.1). Because $\mathbf{R} = (x' - x)\hat{\mathbf{x}} + (y' - y)\hat{\mathbf{y}} + (z' - z)\hat{\mathbf{z}}$ and $\mathbf{R}^\star = (x' - x)\hat{\mathbf{x}} + (y' - y)\hat{\mathbf{y}} + (z' + z)\hat{\mathbf{z}}$ are image points with respect to $z' = 0$, the Green function we seek is

$$G(\mathbf{r}', \mathbf{r}) = \frac{\exp(ik_0 R)}{4\pi R} - \frac{\exp(ik_0 R^\star)}{4\pi R^\star}. \tag{21.77}$$

Now, the z'-derivative of (21.77) evaluated at $z' = 0$ is proportional to the z-derivative of (21.76) evaluated at $z' = 0$. Therefore, if $s^2 = (x' - x)^2 + (y' - y)^2 + z^2$, using (21.77) to evaluate (21.75) gives what is often called the *Rayleigh-Sommerfeld diffraction integral*:

$$u(\mathbf{r}) = -2 \int_{z'=0} dS' \, u(\mathbf{r}') \, \hat{\mathbf{z}} \cdot \nabla G_0 = -\frac{1}{2\pi} \int_{z'=0} dS' \, u(\mathbf{r}') \frac{\partial}{\partial z} \left[\frac{\exp(ik_0 s)}{s} \right]. \tag{21.78}$$

The integral equation (21.78) relates the unique solution of the scalar Helmholtz equation (21.24) in the $z > 0$ half-space to its boundary values $u(x, y, 0)$. Of course, the latter are generally not known.

The name Kirchhoff is associated with an approximation which transforms (21.78) into a formula for $u(\mathbf{r})$. Let $u_0(\mathbf{r})$ be the *incident* plane wave. In Figure 21.15, the idea is to set $u(x, y, 0) = 0$ on the screen and $u(x, y, 0) = u_0(x, y, 0)$ in the aperture. We thereby restrict the integration in (21.78) to the aperture. This is a high-frequency, small-wavelength approximation which performs best when the majority of the field in the aperture is far from the perturbation induced by the boundary of the aperture, in other words, when $\lambda/a \ll 1$ where λ is the wavelength and a is the smallest characteristic dimension of the aperture. This is the usual domain of optics, which was the class of problems of interest to Kirchhoff.

The name Fraunhofer is associated with the far-field limit of (21.78) where $k_0 r \gg 1$. In that case, the z-derivative in (21.78) may be approximated by the multiplicative factor ik_0 and the rightmost integral in (21.78) becomes a mathematical expression of *Huygens' principle*: a wave incident on an

aperture propagates into the far field as if every element of the aperture is the source of a spherical wave with an amplitude and phase given by the incident wave. If, in addition, the aperture size is small and we restrict ourselves to observation points not far from the z-axis, it is common to define a variable $\mathbf{p} = k_0\hat{\mathbf{r}}$, use the far-field limit of ∇G_0 [see (21.97)], and ignore the angular factor $\hat{\mathbf{z}} \cdot \hat{\mathbf{r}}$ to write

$$u(\mathbf{r}) \approx -\frac{ik_0}{2\pi}\frac{\exp(ik_0 r)}{r}\int\limits_{\text{aperture}} dS' u_0(\mathbf{r}')\exp(-i\mathbf{p}\cdot\mathbf{r}'). \tag{21.79}$$

The subject of Fourier optics exploits the conclusion from (21.79) that the far-zone field field $u(x, y, z)$ is proportional to the two-dimensional Fourier transform of the aperture field $u_0(x, y, 0)$.

Further progress requires that we relate the scalar field $u(\mathbf{r})$ to a specific electromagnetic quantity. The Cartesian components of $\mathbf{E}(\mathbf{r})$ and $\mathbf{B}(\mathbf{r})$ are natural choices because each one individually satisfies (21.24) in the $z > 0$ half-space. Unfortunately, the fields obtained by solving the integral equation (21.78) exactly for each component do not generally satisfy the Maxwell equations.[12] This fact notwithstanding, widespread practice simply compares $|u(\mathbf{r})|^2$ with the measured intensity of the field. Figure 21.16 is an example which compares experiment (left side) with the prediction of (21.78) using Kirchhoff's approximation (right side) for a plane wave that diffracts from a circular aperture (radius a) in a plane screen at normal incidence.

The three panels plot the field intensity in planes parallel to the screen for different values of $F = a^2/\lambda z$. When F is an integer and $\lambda/a \ll 1$ (as is the case here) the diffraction pattern in each plane has F maxima and $F - 1$ minima. These features arise from the constructive and destructive interference of waves that arrive at the observation plane from different points in the aperture. The same interference produces oscillating intensity maxima and minima on the symmetry axis ($r = 0$) as a function of F. The agreement between experiment and scalar diffraction theory in Figure 21.16 is remarkable and various explanations of this fact have been offered. All of these draw on the vector theory of electromagnetic diffraction, to which we turn next.[13]

21.8.2 Vector Diffraction Theory

Vector diffraction theory treats the incident field in Figure 21.15 as an electromagnetic plane wave and seeks the unique solution to the Maxwell equations which propagates into the $z > 0$ half-space subject to suitable boundary conditions on the screen and at infinity. There is more than one way to do this. One approach, indicated schematically on the left side of Figure 21.17, exploits the angular spectrum of plane waves (Section 16.6.1) to represent the field at every point in the aperture as an appropriate linear combination of plane waves. The interference of these waves in the near zone (close to the aperture) evolves, in the far zone, to a radiation field determined by the single plane which propagates in the direction $\mathbf{r}$ of observation.

The right side of Figure 21.17 illustrates a different approach to the vector diffraction problem. Here, one generalizes the Huygens' principle idea mentioned in the paragraph preceding (21.79) and regards each point in the aperture as the source of a single *vector* spherical wave. The field at all distances reflects the interference among all the sources. The plane wave and spherical wave points of view provide complementary intuition about the phenomenon of diffraction. In this section, we begin with the plane wave method and describe how it is used to calculate the electric field diffracted by a planar aperture. However, rather than using it to analyze any particular aperture geometry, wesum over

[12] The Sommerfeld half-plane problem (Figure 21.14) has enough symmetry that complete knowledge of one particular field component is sufficient (through the Maxwell equations) to determine all the other components. In that case, $u(\mathbf{r})$ may be identified with that one particular component.

[13] We discuss the apparent success of scalar diffraction theory seen here in Section 21.8.3 below.

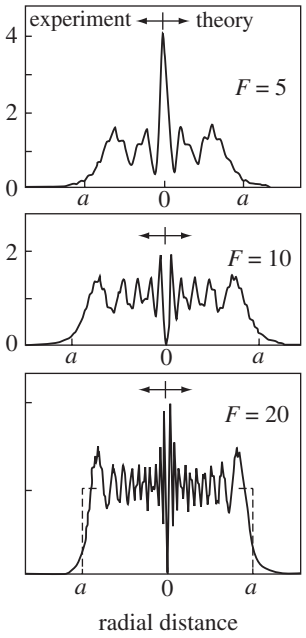

Figure 21.16: Normal-incidence diffraction from a circular aperture of radius a for different values of $F = a^2/\lambda z$. Left: Measured field intensity. Right: $|u(\rho, z)|^2$ calculated using (21.78) and Kirchhoff's approximation. The dashed rectangle is the geometrical optics approximation. Figure from Siegman (1986).

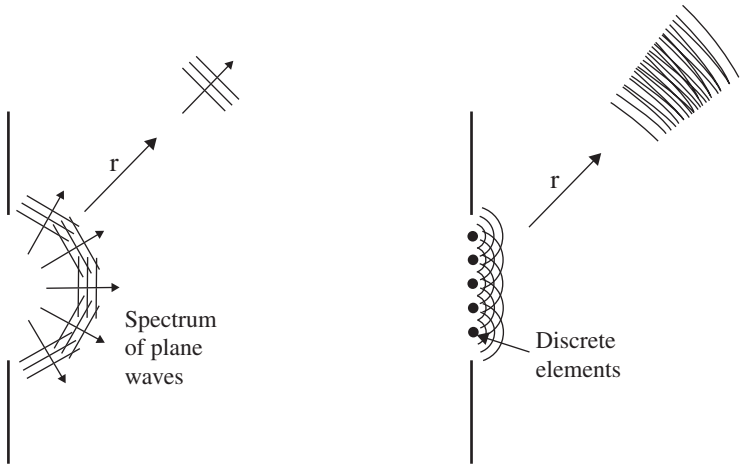

Figure 21.17: Two representations of the field diffracted by an aperture. Left: angular spectrum of plane waves. Right: Huygens' effective sources. Figure from Smith (1997).

the spectrum of plane waves to derive an expression for the diffracted electric field which manifestly illustrates Huygens' principle. Using the latter, we rationalize the success of scalar diffraction theory in Figure 21.16 and calculate the vector fields diffracted by a circular aperture.

Assume that all fields vary as $\exp(-i\omega t)$ and let $\omega = ck_0$. The angular-spectrum approach to diffraction from a planar aperture at $z = 0$ superposes plane wave solutions of the vector Helmholtz

equation,

$$(\nabla^2 + k_0^2)\mathbf{E} = 0, \tag{21.80}$$

in such a way that the sum converges for $z \geq 0$. For a representative plane wave, $\exp(i\mathbf{k}\cdot\mathbf{r})$, these two conditions constrain the wave vector $\mathbf{k} = k_x\hat{\mathbf{x}} + k_y\hat{\mathbf{y}} + k_z\hat{\mathbf{z}}$, so

$$k_z = \begin{cases} \sqrt{k_0^2 - k_x^2 - k_y^2} & k_x^2 + k_y^2 \leq k_0^2, \\ i\sqrt{k_x^2 + k_y^2 - k_0^2} & k_x^2 + k_y^2 \geq k_0^2. \end{cases} \tag{21.81}$$

The plane waves with k_z real in (21.81) propagate with undiminished amplitude as z increases; the waves with k_z imaginary are evanescent and decay exponentially as z increases. In all that follows, it is important to interpret every appearance of the variable k_z (either explicitly or as a component of $\mathbf{k}$) as a shorthand for (21.81).

It is straightforward to construct a sum over plane waves for $\mathbf{E}(x, y, z \geq 0)$ which satisfies $\nabla\cdot\mathbf{E} = 0$ automatically. The key is to make the expansion coefficients the Cartesian components of a two-dimensional vector function $\boldsymbol{\mathcal{E}}(k_x, k_y) = \mathcal{E}_x(k_x, k_y)\hat{\mathbf{x}} + \mathcal{E}_y(k_x, k_y)\hat{\mathbf{y}}$. Doing this, an expression with manifestly zero divergence is

$$\mathbf{E}(x, y, z \geq 0) = \frac{1}{(2\pi)^2}\int_{-\infty}^{\infty} dk_x \int_{-\infty}^{\infty} dk_y \left[\boldsymbol{\mathcal{E}} - \frac{1}{k_z}(\mathbf{k}\cdot\boldsymbol{\mathcal{E}})\,\hat{\mathbf{z}}\right]\exp(i\mathbf{k}\cdot\mathbf{r}). \tag{21.82}$$

It is essential to the completeness of the Fourier representation that (21.82) includes the evanescent waves in (21.81). It does not matter that these waves never reach the far zone. What matters is that their presence in (21.82) influences the amplitudes of the propagating waves in the sum which *do* reach the radiation zone. Now, let $\mathbf{k}_\perp = k_x\hat{\mathbf{x}} + k_y\hat{\mathbf{y}}$ and $\mathbf{r}_\perp = x\hat{\mathbf{x}} + y\hat{\mathbf{y}}$. Equation (21.82) shows that the x- and y-components of the electric field evaluated at $z = 0$ are

$$E_{x,y}(\mathbf{r}_\perp, z = 0) = \frac{1}{2\pi^2}\int d^2k_\perp \mathcal{E}_{x,y}(\mathbf{k}_\perp)\exp(i\mathbf{k}_\perp\cdot\mathbf{r}_\perp). \tag{21.83}$$

Equation (21.83) is a two-dimensional Fourier transform. Therefore, the expansion coefficients we seek are determined by the inverse Fourier transform. Dropping the explicit $z = 0$ on the left side of (21.83), the result is

$$\mathcal{E}_{x,y}(\mathbf{k}_\perp) = \int d^2r'_\perp E_{x,y}(\mathbf{r}'_\perp)\exp(-i\mathbf{k}_\perp\cdot\mathbf{r}'_\perp). \tag{21.84}$$

Substituting (21.84) into (21.82) expresses $\mathbf{E}(x, y, z \geq 0)$ in terms of its transverse components evaluated at $z = 0$. If the solution of this integral equation can be found (or approximated), the associated magnetic field follows from $\nabla\times\mathbf{E} = i\omega\mathbf{B}$.

Practical diffraction calculations using the angular-spectrum method require (i) a guess for the (generally unknown) values of $E_{x,y}(x, y, z = 0)$; (ii) evaluation of the integral (21.84) to find the expansion coefficients; and (iii) evaluation of the field integral (21.82). The reader may wish to explore this approach for specific aperture geometries. Our choice is to bypass such calculations and, instead, transform the sum over plane waves (21.82) into a sum over spherical waves. The calculation proceeds most smoothly if we replace (21.83) by

$$\hat{\mathbf{z}}\times\mathbf{E}(x, y, z = 0) = \frac{1}{(2\pi)^2}\int d^2k_\perp\,[\hat{\mathbf{z}}\times\boldsymbol{\mathcal{E}}(\mathbf{k}_\perp)]\exp(i\mathbf{k}_\perp\cdot\mathbf{r}). \tag{21.85}$$

The associated inverse Fourier transform replaces (21.84):

$$\hat{\mathbf{z}} \times \boldsymbol{\mathcal{E}}(\mathbf{k}_\perp) = \int d^2 r'_\perp \, [\hat{\mathbf{z}} \times \mathbf{E}(\mathbf{r}'_\perp)] \exp(-i\mathbf{k}_\perp \cdot \mathbf{r}'_\perp). \tag{21.86}$$

Our strategy is to exploit (21.86) and a brief, explicit calculation confirms that (21.82) is identical to

$$\mathbf{E}(x, y, z \geq 0) = \frac{i}{(2\pi)^2} \nabla \times \int d^2 k_\perp \left[\frac{\hat{\mathbf{z}} \times \boldsymbol{\mathcal{E}}(\mathbf{k}_\perp)}{k_z} \right] \exp(i\mathbf{k} \cdot \mathbf{r}). \tag{21.87}$$

Substituting (21.86) into (21.87) gives the key intermediate result,

$$\mathbf{E}(\mathbf{r}_\perp, z \geq 0) = \nabla \times 2 \int d^2 r'_\perp \, [\hat{\mathbf{z}} \times \mathbf{E}(\mathbf{r}'_\perp)] \left\{ \frac{i}{8\pi^2} \int \frac{d^2 k_\perp}{k_z} \exp[i\mathbf{k}_\perp \cdot (\mathbf{r} - \mathbf{r}') + ik_z z] \right\}. \tag{21.88}$$

The quantity in curly braces in (21.88) may be rewritten using *Weyl's identity*,[14]

$$\frac{\exp(ik_0 r)}{4\pi r} = \frac{i}{8\pi^2} \int \frac{d^2 k_\perp}{k_z} \exp(i\mathbf{k}_\perp \cdot \mathbf{r}_\perp + ik_z |z|). \tag{21.89}$$

Therefore, because the left side of (21.89) is the free-space Green function (21.76), (21.88) becomes *Smythe's formula* for the diffracted electric field,[15]

$$\mathbf{E}(\mathbf{r}_\perp, z \geq 0) = \nabla \times 2 \int_{z'=0} d^2 r'_\perp \, [\hat{\mathbf{z}} \times \mathbf{E}(\mathbf{r}'_\perp)] G_0(\mathbf{r}, \mathbf{r}'_\perp). \tag{21.90}$$

Equation (21.90) is the vector analog of the scalar integral equation (21.78). The associated magnetic field follows from $\nabla \times \mathbf{E} = i\omega\mathbf{B}$. A precisely analogous calculation gives

$$\mathbf{B}(\mathbf{r}_\perp, z \geq 0) = \nabla \times 2 \int_{z'=0} d^2 r'_\perp \, [\hat{\mathbf{z}} \times \mathbf{B}(\mathbf{r}'_\perp)] G_0(\mathbf{r}, \mathbf{r}'_\perp), \tag{21.91}$$

with an electric field given by $\nabla \times \mathbf{B} = -i\omega\mathbf{E}/c^2$.

A glance back at Application 16.2 of Section 16.9.2 shows that (21.90) and (21.91) are superpositions of the fields (16.183) and (16.184) with harmonic time dependence and different choices for the direction of the constant vector $\hat{\mathbf{s}}$ in the plane of the screen. Taken together, the results of this section show that it is sufficient to know the tangential components of $\mathbf{E}(x, y, z = 0)$ *or* $\mathbf{B}(x, y, z = 0)$ to compute both fields in the $z \geq 0$ half-space. This is consistent with the uniqueness theorem for time-dependent fields (Application 15.1 of Section 15.4.1). It remains only to explore the approximations and limits needed to evaluate (21.90) and (21.91) for practical calculations of the fields diffracted by an aperture in a planar screen.

21.8.3 The Kirchhoff Approximation

The boundary values of $\hat{\mathbf{z}} \times \mathbf{E}$ and $\hat{\mathbf{z}} \times \mathbf{B}$ in (21.90) and (21.91) are generally not known. To make progress, the *Kirchhoff approximation* for this vector problem puts $\mathbf{F} = \mathbf{E}$ in (21.90), $\mathbf{F} = \mathbf{B}$ in (21.91),

[14] The Weyl identity, which makes use of (21.81), can be established by (i) Fourier transforming (21.71) with $\mathbf{r}' = 0$; (ii) solving the resulting algebraic equation for $G(\mathbf{k})$; and (iii) performing the k_z integration of the inverse Fourier transform by contour integration. For a method which avoids the complex plane, see A.S. Marathay, "Fourier transform of the Green function for the Helmholtz equation", *Journal of the Optical Society of America* **65**, 964 (1975).

[15] See W.R. Smythe, "The double current sheet in diffraction", *Physical Review* **72**, 1066 (1947), and Section 12.18 of W.R. Smythe, *Static and Dynamic Electricity*, 3rd edition (McGraw Hill, New York, 1969).

and supposes that

$$\begin{aligned} \hat{\mathbf{z}} \times \mathbf{F} &\approx 0 \ \text{ on the screen } S \\ \hat{\mathbf{z}} \times \mathbf{F} &\approx \hat{\mathbf{z}} \times \mathbf{F}_{\text{inc}} \ \text{ in the aperture } A. \end{aligned} \tag{21.92}$$

This approximation is used for screens of all types in the high-frequency (optical) limit when the wavelength is small compared to the aperture size. As mentioned earlier, this is the regime where the perturbation to the field in the aperture by the aperture boundary should be negligible.[16]

The first line of the Kirchhoff approximation in (21.92) limits the domain of integration in (21.90) and (21.91) to the aperture. This and the spherical wave character of $G_0(\mathbf{r}, \mathbf{r}')$ in (21.76) show that (21.89) and (21.90) reflect the Huygens' principle point of view illustrated on the right side of Figure 21.17, namely, that each point in the aperture is the origin of a spherical wave with a phase and amplitude determined by the incident field.

It is worth noting that, whether one uses $\hat{\mathbf{n}} \times \mathbf{E}$ data or $\hat{\mathbf{n}} \times \mathbf{B}$ data, one of the two Kirchhoff boundary conditions is always *exact* when the screen is an infinitely thin perfect conductor. In that case,

$$\begin{aligned} \hat{\mathbf{z}} \times \mathbf{E} &= 0 \ \text{ on the screen } S \\ \hat{\mathbf{z}} \times \mathbf{B} &= \hat{\mathbf{z}} \times \mathbf{B}_{\text{inc}} \ \text{ in the aperture } A. \end{aligned} \tag{21.93}$$

The first condition is familiar from all our previous work with perfect conductors. The second follows from the surface current density matching condition, $\hat{\mathbf{n}}_2 \times [\mathbf{B}_1 - \mathbf{B}_2] = \mu_0 \mathbf{K}$, and the invariance of the screen with respect to reflection in the $z = 0$ plane. The latter implies that $\hat{\mathbf{z}} \times \mathbf{B}_{\text{ind}}(0^+) = -\hat{\mathbf{z}} \times \mathbf{B}_{\text{ind}}(0^-)$, where $\mathbf{B}_{\text{ind}}$ is the field produced by the currents induced in the screen by the incident field. We conclude that $\hat{\mathbf{z}} \times \mathbf{B}_{\text{ind}}(0^{\pm}) \propto \mathbf{K}$. The current density is zero in the aperture, so only the incident plane wave contributes to $\hat{\mathbf{z}} \times \mathbf{B}(0^+)$.

We now return to Figure 21.16. The Kirchhoff approximation to scalar diffraction theory was used to compute the "theory" half of that figure and our vector diffraction theory will help rationalize the agreement between that theory and experiment. The first step is to perform the curl operation in (21.90). This puts Smythe's formula in the form

$$\mathbf{E}(\mathbf{r}_\perp, z \geq 0) = -2 \int_{z'=0} d^2 r'_\perp \, [\hat{\mathbf{z}} \times \mathbf{E}(\mathbf{r}'_\perp)] \times \nabla G_0(\mathbf{r}, \mathbf{r}'_\perp). \tag{21.94}$$

The second step writes out the cross products in (21.94) to get

$$\mathbf{E}(\mathbf{r}) = -2 \int_{z'=0} d^2 r'_\perp \, \mathbf{E} \, \hat{\mathbf{z}} \cdot \nabla G_0 + 2 \, \hat{\mathbf{z}} \int_{z'=0} d^2 r'_\perp \, \mathbf{E} \cdot \nabla G_0. \tag{21.95}$$

Comparing (21.95) to (21.78) shows that the latter reproduces the former exactly for the field components $E_x(\mathbf{r})$ and $E_y(\mathbf{r})$, but fails to do this for $E_z(\mathbf{r})$. Therefore, the scalar theory should predict experimental field intensities well when E_z is negligible. This is true when the angle of incidence is near normal and the observation points are not far from the symmetry axis (except when $z < \lambda$). These conditions happen to be satisfied for the data shown in Figure 21.16.

21.8.4 Fraunhofer Diffraction

The term *Fraunhofer diffraction* is used when the distance from the aperture to the observation point is large compared to the wavelength and large compared to the size of the aperture. The exact electric

[16] The Kirchhoff approximation can be used to study scattering from a two-dimensional scatterer like a disk or a strip by regarding the plane of the scatterer as "mostly aperture".

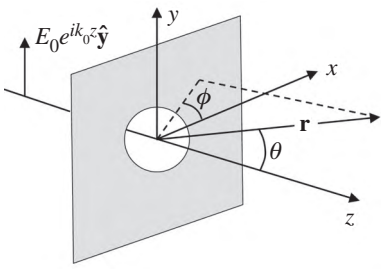

Figure 21.18: Diffraction of a plane wave by a circular aperture.

field expression (21.94) simplifies considerably in this limit. If $\mathbf{R} = \mathbf{r} - \mathbf{r}'$, a brief calculation confirms that the gradient of the free-space Green function (21.76) is

$$\nabla G_0 = (ik_0 R - 1)\frac{G_0(R)}{R}\hat{\mathbf{R}}. \tag{21.96}$$

The stated conditions imply that $k_0 R \gg 1$ and $r \gg r'$. Therefore,

$$\nabla G_0 \approx ik_0 \hat{\mathbf{r}} \frac{\exp(ik_0 r)}{4\pi r} \exp(-ik_0 \hat{\mathbf{r}} \cdot \mathbf{r}'). \tag{21.97}$$

Substituting (21.97) into (21.94) gives the Fraunhofer limit of Smythe's formula as

$$\mathbf{E}_{\text{rad}}(\mathbf{r}_\perp, z \geq 0) = ik_0 \frac{\exp(ik_0 r)}{2\pi r}\hat{\mathbf{r}} \times \int\limits_{z'=0} d^2 r'_\perp \left[\hat{\mathbf{z}} \times \mathbf{E}(\mathbf{r}'_\perp)\right] \exp(-ik_0 \hat{\mathbf{r}} \cdot \mathbf{r}'_\perp). \tag{21.98}$$

As expected for a radiation field, $\mathbf{E}_{\text{rad}}$ is transverse to $\hat{\mathbf{r}}$ and decreases as $1/r$. The asymptotic ($r \to \infty$) magnetic field calculated from $\mathbf{B} = (\nabla \times \mathbf{E})/i\omega$ also has the anticipated radiation zone form,

$$c\mathbf{B}_{\text{rad}} = \hat{\mathbf{r}} \times \mathbf{E}_{\text{rad}}. \tag{21.99}$$

As an example, we consider the Kirchhoff approximation to (21.98) when a normal-incidence plane wave with $\mathbf{E}_{\text{inc}} = E_0 \exp(ik_0 z)\hat{\mathbf{y}}$ strikes a conducting screen with a circular aperture. The screen in Figure 21.18 occupies $z = 0$ and the origin-centered aperture has radius a. The z-axis is normal to the aperture, so $\mathbf{r} = r\sin\theta\cos\phi\,\hat{\mathbf{x}} + r\sin\theta\sin\phi\,\hat{\mathbf{y}} + r\cos\theta\,\hat{\mathbf{z}}$ defines a spherical coordinate system. In the plane of the aperture ($\theta = \pi/2$), we write $\mathbf{r}_\perp = \rho\cos\phi\,\hat{\mathbf{x}} + \rho\sin\phi\,\hat{\mathbf{y}}$. Using these and the formulae in Section 1.2.3,

$$\hat{\mathbf{r}} \times [\hat{\mathbf{z}} \times \mathbf{E}_{\text{inc}}]_{z=0} = -E_0(\sin\phi\hat{\boldsymbol{\theta}} + \cos\phi\cos\theta\hat{\boldsymbol{\phi}}) \quad \text{and} \quad \hat{\mathbf{r}} \cdot \mathbf{r}' = \rho'\sin\theta\cos(\phi - \phi'). \tag{21.100}$$

Therefore,

$$\mathbf{E} = -ik_0 E_0 \frac{\exp(ik_0 r)}{2\pi r}(\sin\phi\hat{\boldsymbol{\theta}} + \cos\phi\cos\theta\hat{\boldsymbol{\phi}}) \int\limits_0^a d\rho'\rho' \int\limits_0^{2\pi} d\phi' \exp[-ik_0\rho'\sin\theta\cos(\phi - \phi')]. \tag{21.101}$$

The symmetry of a circle implies that all the ϕ dependence of the diffracted field is carried by the vector pre-factor in (21.101). Therefore, we can set $\phi = 0$ inside the ϕ integral and use

$$\int\limits_0^{2\pi} d\phi' \exp[-ik_0\rho'\sin\theta\cos\phi'] = 4\int\limits_0^{\pi/2} d\phi' \cos[k_0\rho'\sin\theta\cos\phi']. \tag{21.102}$$

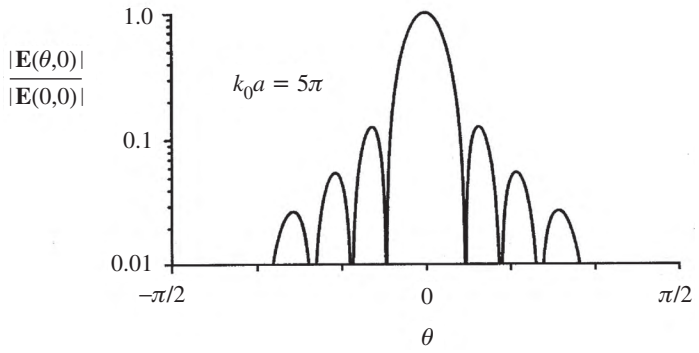

Figure 21.19: Angular dependence of the electric field magnitude diffracted by a circular aperture with $k_0a = 5\pi$. Figure from Smith (1997).

The final result takes a convenient form if we combine (21.102) with an integral representation of the zero-order Bessel function,

$$J_0(u) = \frac{2}{\pi}\int_0^{\pi/2} d\phi \cos(u\cos\phi), \tag{21.103}$$

and the definite integral,

$$\int_0^z du\, u J_0(u) = z J_1(z), \tag{21.104}$$

namely,

$$\mathbf{E}(r,\theta,\phi) = -\frac{i}{2}E_0(k_0a)^2\frac{\exp(ik_0r)}{k_0r}\left[\frac{2J_1(k_0a\sin\theta)}{k_0a\sin\theta}\right](\sin\phi\hat{\boldsymbol{\theta}} + \cos\phi\cos\theta\hat{\boldsymbol{\phi}}). \tag{21.105}$$

Figure 21.19 plots the normalized magnitude of the diffracted electric field (21.105) in the $\phi = 0$ plane for an electrically large aperture with $k_0a = 5\pi$. The vertical scale is logarithmic, so the vast majority of the diffracted field is contained in the central lobe around the forward ($\theta = 0$) direction. The number of side lobes and interference zeroes increases as k_0a increases because they are determined by the zeroes of J_1.

The secondary maxima and minima occur in Figure 21.19 for the same reason they occur in Figure 21.16: constructive and destructive interference among Huygens' wavelets emanating from different points in the aperture. Indeed, a scalar diffraction calculation leads to the same integral that appears in (21.101). For this particular problem, the full Maxwell formalism adds only the vector post-factor in (21.105). On the other hand, the alert reader will have noticed the distinct similarity between the circular aperture diffraction pattern in Figure 21.19 and the radiation pattern for the circular reflector shown in the rightmost panel of Figure 21.12. This is so because the plane represented by the straight line in the middle panel of Figure 21.12 may be regarded as the "aperture" in a "screen" which happens to be made of vacuum. The field reflected from the concave dish onto this circular aperture serves as the "incident" field in a Kirchhoff/Fraunhofer approximation to the field radiated by the reflector.

We conclude with a brief historical remark. Lord Rayleigh famously used the scalar version of (21.105) to determine the resolving power of a telescope or microscope with a circular aperture. He suggested that two point sources are just resolvable if their angular separation θ is such that the first

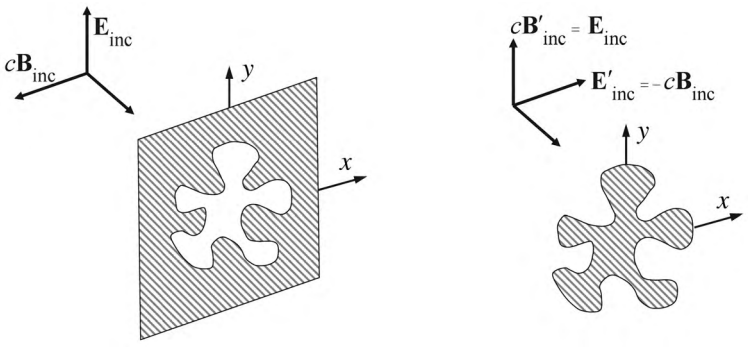

Figure 21.20: Plane wave scattering from an aperture in a conducting screen (left panel) and from a complementary conducting plate (right panel).

minimum of the diffraction pattern of one source coincides with the central maximum of the diffraction pattern of the other source. Since $x_1 = 3.832$ is the first zero of $J_1(x)$, we set $k_0 a \sin\theta = x_1$ and use $\lambda = 2\pi/k_0$ to write the *Rayleigh criterion* as

$$\sin\theta = 0.6\,\frac{\lambda}{a}. \tag{21.106}$$

21.9 Generalized Optical Principles

Before Maxwell, the laws of optics were developed using a scalar field (the light intensity or its square root) as the fundamental quantity. After Maxwell, the optical laws were generalized to be consistent with the vector field theory of electromagnetism. The previous section presented an example: a Huygens-like principle for the electric and magnetic fields diffracted by an aperture cut out of an infinite planar sheet. In this section, we specialize to an aperture cut out of a *conducting* sheet and prove an electromagnetic version of Babinet's principle. We then return to Huygens' principle and prove a vector version of the principle for the electric and magnetic fields diffracted by an *arbitrary* scatterer.

21.9.1 Babinet's Principle for Vector Fields

Babinet's principle elegantly relates the scattering produced by the two *complementary* objects shown in Figure 21.20. One is a flat, infinitely large, infinitesimally thin, and perfectly conducting sheet with an aperture cut out. The other is a flat, infinitesimally thin, and perfectly conducting plate with the exact size and shape of the aperture. The incident plane waves in the two cases are not identical. Rather,

$$\mathbf{E}'_{\text{inc}} = -c\mathbf{B}_{\text{inc}} \qquad \text{and} \qquad c\mathbf{B}'_{\text{inc}} = \mathbf{E}_{\text{inc}}. \tag{21.107}$$

The total fields in each case are the sum of the incident fields shown and the field scattered by each conductor. Thus,

$$\mathbf{B} = \mathbf{B}_{\text{inc}} + \mathbf{B}_{\text{scatt}} \qquad \text{and} \qquad \mathbf{E} = \mathbf{E}_{\text{inc}} + \mathbf{E}_{\text{scatt}}, \tag{21.108}$$

and similarly for the primed fields. Babinet's principle asserts that the electromagnetic fields of these complementary scattering problems are related by

$$\mathbf{E}'_{\text{scatt}} = c\mathbf{B} \qquad \text{and} \qquad c\mathbf{B}'_{\text{scatt}} = -\mathbf{E}. \tag{21.109}$$

We prove (21.109) by writing out the time-harmonic ($\omega = ck_0$) Maxwell equations and the boundary conditions satisfied by $(\mathbf{E}, \mathbf{B})$ and by $(\mathbf{E}'_{\text{scatt}}, \mathbf{B}'_{\text{scatt}})$. For the aperture problem, the total field in the $z > 0$ half-space satisfies

$$\nabla \times \mathbf{E} = ik_0(c\mathbf{B}) \qquad \text{and} \qquad \nabla \times (c\mathbf{B}) = -ik_0\mathbf{E}. \tag{21.110}$$

We repeat from (21.93) the boundary conditions for the total field at $z = 0$:

$$\begin{aligned} \hat{\mathbf{z}} \times \mathbf{E} &= 0 \qquad\qquad \text{off the aperture} \\ \hat{\mathbf{z}} \times \mathbf{B} &= \hat{\mathbf{z}} \times \mathbf{B}_{\text{inc}} \qquad \text{on the aperture.} \end{aligned} \tag{21.111}$$

For the plate problem, the scattered field in the $z > 0$ half-space satisfies

$$\nabla \times \mathbf{E}'_{\text{scatt}} = ik_0(c\mathbf{B}'_{\text{scatt}}) \qquad \text{and} \qquad \nabla \times (c\mathbf{B}'_{\text{scatt}}) = -ik_0\mathbf{E}'_{\text{scatt}}. \tag{21.112}$$

The boundary conditions for the scattered field at $z = 0$ are

$$\begin{aligned} \hat{\mathbf{z}} \times (c\mathbf{B}'_{\text{scatt}}) &= 0 \qquad\qquad \text{off the plate} \\ \hat{\mathbf{z}} \times \mathbf{E}'_{\text{scatt}} &= \hat{\mathbf{z}} \times (c\mathbf{B}_{\text{inc}}) \qquad \text{on the plate.} \end{aligned} \tag{21.113}$$

The first condition in (21.113) is true for the same reason that the second condition in (21.111) is true. The second condition in (21.113) follows from $\hat{\mathbf{z}} \times (\mathbf{E}'_{\text{scatt}} + \mathbf{E}'_{\text{inc}}) = 0$ and (21.107). This is all we need. Babinet's principle (21.109) is the statement that (21.112) and (21.113) transform to (21.110) and (21.111) when we make the duality substitutions $\mathbf{E}'_{\text{scatt}} \to c\mathbf{B}$ and $c\mathbf{B}'_{\text{scatt}} \to -\mathbf{E}$.[17] We emphasize that Babinet's principle (21.109) is an *exact* result which applies to both the near-field and far-field limits of the scattered fields.

A straightforward application of Babinet's principle relates the diffraction pattern produced by a circular hole in a conducting sheet to the diffraction pattern produced by a conducting disk which just fills the hole. Because $(\hat{\mathbf{k}}, \mathbf{E}_{\text{rad}}, \mathbf{B}_{\text{rad}})$ forms a right-handed orthogonal triad of vectors and $|\mathbf{E}| = c|\mathbf{B}|$ in the radiation zone, the cross product of $\hat{\mathbf{k}}$ with (21.109) evaluated in the radiation zone gives

$$\begin{aligned} \hat{\mathbf{k}} \times \mathbf{E}_{\text{rad}}(\text{disk}) = \hat{\mathbf{k}} \times c\mathbf{B}_{\text{rad}}(\text{hole}) \quad &\Longrightarrow \quad c\mathbf{B}_{\text{rad}}(\text{disk}) = -\mathbf{E}_{\text{rad}}(\text{hole}) \\ \hat{\mathbf{k}} \times c\mathbf{B}_{\text{rad}}(\text{disk}) = -\hat{\mathbf{k}} \times \mathbf{E}_{\text{rad}}(\text{hole}) \quad &\Longrightarrow \quad \mathbf{E}_{\text{rad}}(\text{disk}) = c\mathbf{B}_{\text{rad}}(\text{hole}). \end{aligned} \tag{21.114}$$

Consequently,

$$|\mathbf{E}_{\text{rad}}(\text{disk})| = |\mathbf{E}_{\text{rad}}(\text{hole})| \qquad \text{and} \qquad |\mathbf{B}_{\text{rad}}(\text{disk})| = |\mathbf{B}_{\text{rad}}(\text{hole})|. \tag{21.115}$$

This tells us that, apart from the difference in incident field polarization implied by (21.107), the far-field diffraction patterns produced by a circular aperture and a conducting disk are the same. For normal incidence, that pattern is Figure 21.19 when the Kirchhoff approximation is valid. The latter replaces the true field by the incident field in the hole, so this will be true only for electrically large apertures where the perturbation from the hole's perimeter can be tolerated.

Application 21.3 Sub-Wavelength Apertures and Near-Field Optics

This application uses Babinet's principle and the physics of the angular-spectrum representation to analyze the diffraction of a plane wave by a sub-wavelength aperture ($a \ll \lambda$) in a conducting sheet. In the *far field*, we will confirm the expectation from Section 21.8.3 that Kirchhoff's approximation fails for an electrically small aperture. In the *near field*, we will learn how to "beat the diffraction limit" set by the Rayleigh criterion (21.106).

[17] See Section 15.2.2 for the duality of free electromagnetic fields.

Our statement about the far field is true because Babinet's principle (see Section 21.9.1) guarantees that the fields transmitted through the aperture into $z > 0$ are related by duality to the fields diffracted into $z > 0$ by a perfectly conducting, two-dimensional object which just fills the hole. But according to Section 21.4, an electrically small object produces Rayleigh scattering with its characteristic λ^{-4} variation of the cross section. This disagrees with the Kirchhoff prediction that $\sigma_{\text{scatt}} \propto \lambda^{-2}$ because the quantity in square brackets in (21.105) approaches one when $k_0 a \ll 1$. In words, the transmission of a plane wave through a very small aperture in a perfect conductor is *very much less* than the Kirchhoff approximation predicts.

The Babinet argument implies that the differential cross section for scattering by a small aperture in a conducting sheet is given by (21.20) if we can compute the electric and magnetic dipole moments induced in the apertured conductor when a long-wavelength plane wave strikes it. Using a quasistatic approximation appropriate to $\lambda \gg a$, we leave it as an exercise for the reader to show that these moments can be calculated directly using the aperture geometry, or indirectly using Babinet's principle and the dipole moments calculated for the flat, conducting object shaped like the aperture.[18] Here, we content ourselves with a qualitative discussion for a plane wave incident on a circular aperture from an arbitrary angle of incidence, as shown in Figure 21.15.

Consider the polarization where $\mathbf{B}_0$ lies parallel to the screen. The conductor boundary condition $\hat{\mathbf{n}} \cdot \mathbf{B}|_S = 0$ ensures that the field line pattern very near the hole looks something like the left panel of Figure 21.21. In the far field, the magnetic field line pattern for $z > 0$ is the same as that produced by a magnetic dipole at the center of the hole oriented anti-parallel to the long-wavelength field incident from $z < 0$. The electric field for this polarization has components both parallel to the screen and perpendicular to the screen. However, the conductor boundary condition $\hat{\mathbf{n}} \times \mathbf{E}|_S = 0$ ensures that the field line pattern very near the hole looks something like the right panel of Figure 21.21. In the far field, the electric field line pattern for $z > 0$ is the same as that produced by an electric dipole at the center of the hole oriented parallel to the long-wavelength field incident from $z < 0$. The other polarization has $\mathbf{E}_0$ parallel to the screen and produces only a magnetic dipole response in the far field.

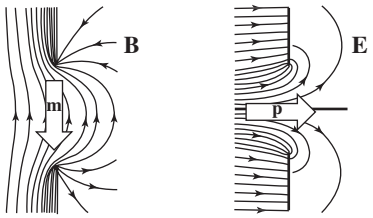

Figure 21.21: Uniform fields induce dipole moments in a metal sheet with an aperture. Left panel: magnetic dipole moment **m**. Right panel: electric dipole moment **p**. Figure adapted from Drezet, Woehl, and Huant (2002).

There is more to learn about the *near field* in the immediate vicinity of a very small aperture than Figure 21.21 suggests. To see this, we exploit the angular-spectrum representation (21.82) of the field diffracted into $z > 0$ by the aperture. The restriction (21.81) is crucial. If a plane wave with $k_x^2 + k_y^2 > \omega^2/c^2$ contributes to the transmitted field, k_z is a positive imaginary number and the plane wave in question does not propagate into the far zone. It is *evanescent* and decays exponentially as z increases.[19] The key observation is that evanescent waves contribute more and more to

[18] For an "elementary" derivation of the dipole moments induced in a conducting disk, see R. Friedberg, "The electrostatics and magnetostatics of a conducting disk", *American Journal of Physics* **61**, 1084 (1993).

[19] Section 17.3.7 reviews the properties of evanescent waves.

the sum (21.82) as the aperture size becomes smaller. This can be understood from our discussion of the complementarity inequality, $\Delta x \Delta k_x \geq \frac{1}{2}$, which connects the spatial size of a wave packet in the x-direction to the spread in wave vectors needed for its Fourier synthesis (see Section 16.5.3). For the present problem, we identify $\Delta x \Delta y$ with the area of an electrically small aperture and conclude that the angular spectrum of any wave it transmits must contain many evanescent waves with large values of k_x and k_y.

The mere fact that far fewer propagating waves contribute to the radiation zone of an electrically small aperture compared to an electrically large aperture is one way to understand the much reduced intensity of Rayleigh scattering compared to Kirchhoff scattering. Similarly, the Rayleigh criterion (21.106) applies only to images formed from propagating waves. It says nothing about the resolution possible for an object which lies so close to a sub-wavelength aperture that it is illuminated principally by evanescent waves. In that case, the main issue is the exponential decay of the waves and a spatial resolution $d \ll \lambda$ can be achieved simply by locating the object within a distance d of the aperture. This is the operating principle behind the field of *near-field optics*. ■

21.9.2 Huygens' Principle for Vector Fields

Let the surface S in Figure 21.22 completely enclose an arbitrary scattering or diffracting object. We take this to mean that the volume Ω contains one or more sources of a time-harmonic electromagnetic field. In this section, we generalize the results of Section 21.8.2 and prove that the scattered or diffracted fields in the volume V outside S can be represented by a set of spherical wave sources distributed over S. The source strengths are determined by the tangential components of $\mathbf{E}$ and $\mathbf{B}$ on S. This is a generalized *Huygens' principle* for electromagnetic fields.

Among the several ways to proceed, we avoid dyadic Green functions and excessive algebra by exploiting a fairly unfamiliar identity of vector calculus.[20] If $\psi(\mathbf{r}')$ is a scalar function, $\mathbf{E}(\mathbf{r}')$ is a vector function, and $\hat{\mathbf{n}}'$ is the unit normal to S that points *into* V,

$$\int_V d^3r' \left[\psi \nabla' \times (\nabla' \times \mathbf{E}) + \mathbf{E}\nabla'^2\psi + (\nabla' \cdot \mathbf{E})\nabla'\psi\right] = -\int_S dS' \left[\psi\, \hat{\mathbf{n}}' \times (\nabla' \times \mathbf{E}) + (\hat{\mathbf{n}}' \times \mathbf{E}) \times \nabla'\psi + (\hat{\mathbf{n}}' \cdot \mathbf{E})\nabla'\psi\right]. \quad (21.116)$$

For our application, the vector $\mathbf{E}(\mathbf{r}')$ is the space part of a time-harmonic electric field with frequency $\omega = ck_0$. In V, this quantity satisfies $\nabla' \cdot \mathbf{E} = 0$, $\nabla' \times \mathbf{E} = i\omega\mathbf{B}$, and $\nabla' \times \nabla' \times \mathbf{E} = k_0^2\mathbf{E}$. The scalar $\psi(\mathbf{r}') = G_0(\mathbf{r}, \mathbf{r}')$ is the free-space Green function (21.76). The latter satisfies (21.71) and goes to zero when either argument goes to infinity. Substituting all this information into (21.116) and choosing $\mathbf{r}$ to lie in the complementary volume Ω gives

$$\mathbf{E}(\mathbf{r} \in \Omega) = 0. \quad (21.117)$$

Choosing $\mathbf{r} \in V$ gives a formula where only integrals over the surface S appear:

$$\mathbf{E}(\mathbf{r} \in V) = i\omega \int_S dS' \,[\hat{\mathbf{n}}' \times \mathbf{B}(\mathbf{r}')]G_0(\mathbf{r}, \mathbf{r}') + \int_S dS' \,[\hat{\mathbf{n}}' \times \mathbf{E}(\mathbf{r}')] \times \nabla' G_0(\mathbf{r}, \mathbf{r}') + \int_S dS' \,[\hat{\mathbf{n}}' \cdot \mathbf{E}(\mathbf{r}')]\nabla' G_0(\mathbf{r}, \mathbf{r}'). \quad (21.118)$$

[20] A one-page paper with a straightforward proof of (21.116) is H. Unz, "Scalar-vector analog of Green's theorem", *IRE Transactions on Antennas and Propagation*, **6**, 300 (1958).

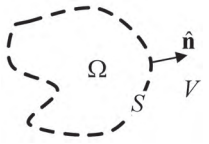

Figure 21.22: Geometry used to discuss Huygens' principle for electromagnetic fields.

A similar calculation replaces $\mathbf{E}$ by $\mathbf{B}$ in (21.116) and uses $\nabla' \cdot \mathbf{B} = 0$, $\nabla' \times \mathbf{B} = -i\omega\mathbf{E}/c^2$, and $\nabla' \times \nabla' \times \mathbf{B} = k_0^2\mathbf{B}$. The result is $\mathbf{B}(\mathbf{r} \in \Omega) = 0$ and

$$\begin{aligned}\mathbf{B}(\mathbf{r} \in V) = -i(k_0/c)\int_S dS'\,[\hat{\mathbf{n}}' \times \mathbf{E}(\mathbf{r}')]G_0(\mathbf{r},\mathbf{r}') + \int_S dS'\,[\hat{\mathbf{n}}' \times \mathbf{B}(\mathbf{r}')] \times \nabla' G_0(\mathbf{r},\mathbf{r}') \\ + \int_S dS'\,[\hat{\mathbf{n}}' \cdot \mathbf{B}(\mathbf{r}')]\nabla' G_0(\mathbf{r},\mathbf{r}').\end{aligned} \tag{21.119}$$

Equations (21.118) and (21.119) are called the *Stratton-Chu formulae*. They are important for situations where the compact volume Ω contains the charge and current and it is necessary to know the details of the fields in the much larger volume V. A typical calculation uses a numerical method to find the solution in Ω and on S, and then substitutes the latter into the Stratton-Chu formulae to get the solution in V. For conceptual purposes, we transform (21.118) and (21.119) as follows: (i) use $\nabla' G_0 = -\nabla G_0$ to bring the gradient operators outside the integrals; (ii) take the curl of each equation; and (iii) use a Maxwell curl equation to eliminate the curl on the left side of each. These operations generate what are called the *Franz formulae*:

$$\begin{aligned}\mathbf{E}(\mathbf{r} \in V) &= \nabla \times \int_S dS'\,[\hat{\mathbf{n}}' \times \mathbf{E}(\mathbf{r}')]G_0(\mathbf{r},\mathbf{r}') + \frac{ic^2}{\omega}\nabla \times \nabla \times \int_S dS'\,[\hat{\mathbf{n}}' \times \mathbf{B}(\mathbf{r}')]G_0(\mathbf{r},\mathbf{r}') \\ \mathbf{B}(\mathbf{r} \in V) &= \nabla \times \int_S dS'\,[\hat{\mathbf{n}}' \times \mathbf{B}(\mathbf{r}')]G_0(\mathbf{r},\mathbf{r}') - \frac{i}{\omega}\nabla \times \nabla \times \int_S dS'\,[\hat{\mathbf{n}}' \times \mathbf{E}(\mathbf{r}')]G_0(\mathbf{r},\mathbf{r}').\end{aligned} \tag{21.120}$$

The Franz formulae are interesting, not least because they require more information than strictly should be necessary. Each involves both $\hat{\mathbf{n}} \times \mathbf{E}|_S$ *and* $\hat{\mathbf{n}} \times \mathbf{B}|_S$, while the uniqueness theorem (mentioned at the end of Section 21.8.2) tells us that only $\hat{\mathbf{n}} \times \mathbf{E}|_S$ *or* $\hat{\mathbf{n}} \times \mathbf{B}|_S$ should be needed. That being said, the only geometry known where an explicit formula exists to compute the fields in a volume when only one tangential field component is known on the boundary is the planar aperture to which (21.90) and (21.91) apply. For all other geometries, both surface quantities must be known or approximated. An example is the physical optics expression (21.52). This may be derived by substituting $\hat{\mathbf{n}} \times \mathbf{E}|_S = 0$ and (21.51) into the right side of (21.120) and then passing to the radiation zone using (21.97) to evaluate the interior curl operation and $\nabla \to i\mathbf{k}$ to evaluate the exterior curl operation.

The physics represented by the Franz formulae becomes clear when we recall (from Section 20.4) the fields produced by an origin-centered point electric dipole with moment $\mathbf{p}(t)$,

$$\mathbf{B}(\mathbf{r},t) = \nabla \times \frac{\mu_0}{4\pi}\frac{\dot{\mathbf{p}}_{\text{ret}}}{r} \qquad \text{and} \qquad \mathbf{E}(\mathbf{r},t) = \nabla \times \nabla \times \frac{1}{4\pi\epsilon_0}\frac{\mathbf{p}_{\text{ret}}}{r}, \tag{21.121}$$

and the fields produced by an origin-centered point magnetic dipole with moment $\mathbf{m}(t)$,

$$\mathbf{E}(\mathbf{r},t) = -\nabla \times \frac{\mu_0}{4\pi}\frac{\dot{\mathbf{m}}_{\text{ret}}}{r} \qquad \text{and} \qquad \mathbf{B}(\mathbf{r},t) = \nabla \times \nabla \times \frac{\mu_0}{4\pi}\frac{\mathbf{m}_{\text{ret}}}{r}. \tag{21.122}$$

We are concerned with time-harmonic sources, so $\mathbf{p}_{\rm ret} = \mathbf{p}(t - r/c) = \mathbf{p}\exp[i(k_0 r - \omega t)]$ and $\mathbf{m}_{\rm ret} = \mathbf{m}(t - r/c) = \mathbf{m}\exp[i(k_0 r - \omega t)]$. In that case, a direct comparison of (21.121) and (21.122) with (21.120) shows that the latter are exactly the fields of a surface S endowed with point electric and magnetic dipoles with areal densities[21]

$$\frac{d\mathbf{p}}{dS} = \frac{i}{\omega\mu_0}\,[\hat{\mathbf{n}} \times \mathbf{B}]_S \qquad \text{and} \qquad \frac{d\mathbf{m}}{dS} = -\frac{i}{\omega\mu_0}\,[\hat{\mathbf{n}} \times \mathbf{E}]_S\,. \tag{21.123}$$

The presence of the free-space Green functions in (21.120) embodies the Huygens'-principle idea that the fields in V may be thought of as produced by effective spherical wave sources distributed over S.

Example 21.4 Show that (21.120) reduces to (21.90) and (21.91) when the volume V in Figure 21.22 is the $z > 0$ half-space. Hint: Compare the fields at $\mathbf{r} = (x, y, z > 0)$ with the fields at the image point $\bar{\mathbf{r}} = (x, y, -z)$.

Solution: The given V identifies the surface S as the $z = 0$ plane and the normal $\hat{\mathbf{n}}' = \hat{\mathbf{z}}$. Using the hint and (21.117), the left side of (21.120) vanishes when the right side is evaluated at the image point $\bar{\mathbf{r}}$, which lies in Ω. Accordingly, the electric field equation reads

$$0 = \nabla \times \int_S dS'\,[\hat{\mathbf{z}} \times \mathbf{E}(\mathbf{r}')]G_0(\bar{\mathbf{r}}, \mathbf{r}') + \frac{ic^2}{\omega}\nabla \times \nabla \times \int_S dS'\,[\hat{\mathbf{z}} \times \mathbf{B}(\mathbf{r}')]G_0(\bar{\mathbf{r}}, \mathbf{r}').$$

Each curl operation refers to the observation point. Therefore, the z-derivative of the gradient operator introduces a minus sign when it acts on $G_0(\bar{\mathbf{r}}, \mathbf{r}')$. Moreover, $G_0(\bar{\mathbf{r}}, \mathbf{r}') = G_0(\mathbf{r}, \mathbf{r}')$ when $z' = 0$. Therefore, the z-component of the first term of the equation just above has the same sign as the corresponding component of (21.120) while the x- and y-components have the opposite sign. Similarly, the z-component of the second term of the null equation has the opposite sign as the corresponding component of (21.120) while the x- and y-components have the same sign. Therefore, adding the z-components of the two equations and subtracting the x- and y-components of the two equations gives the advertised result,

$$\mathbf{E}(x, y, z > 0) = \nabla \times 2 \int_S dS'\,[\hat{\mathbf{z}} \times \mathbf{E}(\mathbf{r}')]G_0(\mathbf{r}, \mathbf{r}').$$

A similar argument reduces the magnetic field equation in (21.120) to (21.91).

Sources, References, and Additional Reading

The quotation at the beginning of the chapter is taken from

V. Fock, "New methods in diffraction theory" *Philosophical Magazine* **39**, 149 (1948).

Section 21.1 *Smith* and *Landau and Lifshitz* treat the subject of this chapter very differently, but with equal clarity and insight. Our debt to the former will be obvious. *Ishimaru* presents many different approaches to scattering and diffraction. *Newton* compares electromagnetic scattering to particle scattering and quantum mechanical wave scattering. The latter two books treat polarization effects in detail.

G.S. Smith, *An Introduction to Classical Electromagnetic Radiation* (University Press, Cambridge, 1997).

[21] Textbooks of engineering electromagnetism often relate $[\hat{\mathbf{n}} \times \mathbf{B}]_S$ to a current of electric charge and $[\hat{\mathbf{n}} \times \mathbf{E}]_S$ to a current of (fictitious) magnetic charge.

L.D. Landau and E.M. Lifshitz, *Electrodynamics of Continuous Media* (Pergamon, Oxford, 1960).

A. Ishimaru, *Electromagnetic Wave Propagation, Radiation, and Scattering* (Prentice-Hall, Upper Saddle River, NJ, 1991).

R.G. Newton, *Scattering Theory of Waves and Particles* (McGraw-Hill, New York, 1966).

Two expert-level treatments of scattering and diffraction are

G.T. Ruck, D.E. Barrick, W.D. Stuart, and C.K. Krichbaum, *Radar Cross Section Handbook* (Plenum, New York, 1970), Volume 1.

M. Nieto-Vesperinas, *Scattering and Diffraction in Physical Optics* (Wiley, New York, 1991).

Figure 21.1 was adapted from

G. Toraldo di Francia, *Electromagnetic Waves* (Wiley-Interscience, New York, 1953).

Section 21.3 Application 21.1 is based on a discussion in

S. Dodelson, *Modern Cosmology* (Academic, Amsterdam, 2003), Chapter 10.

Section 21.4 *Smith* discusses dipole scattering from small particles, its role in the human perception of atmospheric color, and the contributions of Rayleigh, Smoluchowski, and Einstein to the theory in

G.S. Smith, "Human color vision and the unsaturated blue color of the daytime sky", *American Journal of Physics* **73**, 590 (2005).

G.S. Smith, "Summing the molecular contributions to skylight", *American Journal of Physics* **76**, 816 (2008).

Section 21.5 Our discussion of scattering from an infinite conducting cylinder follows *Egyes*. The classic reference on Mie scattering from dielectric spheres is by *van de Hulst*. The treatise by *Grandy* brings his discussion up to date. *Ruck et al.* (see Section 21.1 above) review the literature of scattering from conducting spheres and cylinders in great detail.

L. Eyges, *The Classical Electromagnetic Field* (Dover, New York, 1972).

H.C. van de Hulst, *Light Scattering by Small Particles* (Wiley, New York, 1957).

W.T. Grandy, Jr., *Scattering of Waves by Large Spheres* (University Press, Cambridge, 2000).

Figure 21.9 was produced by MiePlot, a code at wwww.philiplaven.com/mieplot.htm. Figure 21.10 comes from

L.G. Guimarães and H.M. Nussenzveig, "Theory of Mie resonances and ripple fluctuations", *Optics Communications* **89**, 363 (1992).

For an appreciation of Ludvig Lorenz, see

O. Keller, "Optical works of L.V. Lorenz", in *Progress in Optics*, vol. 43 (Elsevier, Amsterdam, 2002), Chapter 3.

Section 21.6 Figure 21.11 was produced using MiePlot (see Section 21.5 above). *Macdonald* gave the first discussion of the physical optics approximation. Figure 21.12 was adapted from *Imbriale*:

H.M. Macdonald, "The effect produced by an obstacle on a train of electric waves", *Philosophical Transactions of the Royal Society of London A* **212**, 299 (1912).

W.A. Imbriale, *Large Antennas of the Deep Space Network* (Wiley-Interscience, New York, 2003), Chapter 9.

Section 21.7 *Newton* gives a short history of the optical theorem. Our proof is due to *Saxon* in the form given by *Mishchenko et al.* The approximation derived in Application 21.2 is due to *van de Hulst* (see Section 21.5 above) in the form given by *Loudec et al.*

R.G. Newton, "Optical theorem and beyond", *American Journal of Physics* **44**, 639 (1976).

D.S. Saxon, "Tensor scattering matrix for the electromagnetic field", *Physical Review* **100**, 1771 (1955).

M.I. Mishchenko, L.D. Travis, and A.A. Lacis, *Scattering, Absorption, and Emission of Light by Small Particles* (University Press, Cambridge, 2002).

K. Louedec, S. Dagoret-Campagne, and M. Urban, "Ramsauer approach to Mie scattering of light on spherical particles", *Physica Scripta* **80**, 35403 (2009).

Van de Hulst (see Section 21.5 above) and *Brillouin* give differing explanations of the extinction paradox. Our discussion follows *Berg et al.*

L. Brillouin, "The scattering cross section of spheres for electromagnetic waves", *Journal of Applied Physics* **20**, 1110 (1949).

M.J. Berg, C.M. Sorensen, and A. Chakrabarti, "A new explanation of the extinction paradox", *Journal of Quantitative Spectroscopy & Radiative Transfer* **112**, 1170 (2011).

Section 21.8 The textbook by *Sommerfeld* describes his exact solution to the electromagnetic diffraction problem for a conducting half-plane. Figure 21.14 comes from *Berry*.

A. Sommerfeld, *Optics* (Academic, New York 1954).

M. Berry, "Geometry of phase and polarization singularities, illustrated by edge diffraction and the tides", in *The Second International Conference on Singular Optics*, edited by M.S. Soskin and M.V. Vasnetsov, Proceedings of the SPIE, vol. 4403 (2001), pp. 1-12.

Most optics textbooks (including *Sommerfeld* above) discuss scalar diffraction theory in more or less detail. *Goodman* is the standard reference for the role of the Fourier transform in far-field diffraction. Figure 21.16 comes from *Siegman*.

J. Goodman, *Introduction to Fourier Optics*, 3rd edition (Roberts and Company, Greenwood Village, CO, 2005).

A.E. Siegman, *Lasers* (University Science Books, Sausalito, CA, 1986), Section 18.4.

Our treatment of vector diffraction theory follows *Smith* (see Section 21.1), which is also the source of Figure 21.17 and Figure 21.19.

Section 21.9 Our proof of Babinet's principle is due to *Smith* (see Section 21.1). *Bethe* is the author of the classic paper on diffraction by small apertures. *Hecht et al.* provide a very readable overview of the field of near-field optics. Figure 21.21 was adapted from *Drezet et al.*

H.A. Bethe, "Theory of diffraction by small holes", *Physical Review* **66**, 163 (1944).

B. Hecht, B. Sick, U.P. Wild, *et al.*, "Scanning near-field optical microscopy with aperture probes: Fundamentals and applications", *Journal of Chemical Physics* **112**, 7761 (2000).

A. Drezet, J.C. Woehl, and S. Huant, "Diffraction by a small aperture in a conical geometry", *Physical Review E* **65**, 46611 (2002).

Our discussion of Huygens' principle and the Franz formulae benefitted from *Tai*. Example 21.4 comes from the mathematically rigorous monograph by *Jones*.

C.-T. Tai, "Kirchhoff theory: Scalar, vector, or dyadic?", *IEEE Transactions on Antennas and Propagation* **20**, 114 (1972).

D.S. Jones, *The Theory of Electromagnetism* (Macmillan, New York, 1964).

Problems

21.1 **Scattering from a Bound Electron** Find the total scattering cross section when a circularly polarized wave scatters from an electron bound to a point in space by a spring with spring constant k. Assume that the amplitude of the incident wave is not large.

21.2 **Scattering from a Hydrogen Atom** Let $\mathbf{q} = \mathbf{k_0} - \mathbf{k}$ be the scattering vector defined in Example 1.2. If a_B is the Bohr radius, show that the cross section for plane wave scattering from a hydrogen atom is proportional to the factor $[1 + (qa_B/2)^2]^{-4}$.

21.3 **Double Scattering** A long-wavelength, left circularly polarized, monochromatic plane wave scatters into the direction $\hat{\mathbf{k}}_1$ from a uniform dielectric sphere with radius a and polarizability α. The scattered wave travels a distance $r_1 \gg a$ and scatters from an identical sphere into the direction $\hat{\mathbf{k}}_2$. Find the twice-scattered electric field at a distance $r_2 \gg a$ from the second sphere. Express your answer using polarization vectors which are (i) transverse to $\hat{\mathbf{k}}_2$ and (ii) parallel and perpendicular to the plane of the diagram.

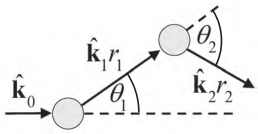

21.4 Rayleigh Scattering à la Rayleigh In one of his papers devoted to the color of skylight, Lord Rayleigh used physical reasoning and dimensional analysis to deduce the wavelength dependence of the intensity of light scattered by a particle in the atmosphere. Invent Rayleigh's argument, beginning with his assumption that the ratio of the scattered field amplitude to the incident field amplitude *could* depend on (i) the volume of the particle, (ii) the distance from the particle to the observation point, (iii) the wavelength of the scattered light, and (iv) the speed of light.

21.5 Rayleigh Scattering from a Conducting Sphere

(a) Place a perfectly conducting sphere with radius a in a uniform electric field $\mathbf{E}_0$ and let an origin-centered electric dipole field represent the field produced by the sphere. Use this information to deduce that $\mathbf{p} = 4\pi\epsilon_0 a^2 \mathbf{E}_0$ is the dipole moment induced in the sphere.

(b) Place the sphere in a uniform magnetic field $\mathbf{B}_0$ and let an origin-centered magnetic dipole field represent the field produced by the sphere. Use this information to deduce that $\mathbf{m} = -(2\pi a^3/\mu_0)\mathbf{B}_0$ is the dipole moment induced in the sphere.

(c) Let θ be the angle between the incident wave vector $\mathbf{k}_0$ and the scattered wave vector $\mathbf{k}$. If $ka \ll 1$, show that the differential cross section for scattering of an unpolarized plane wave by the perfectly conducting sphere is

$$\left\langle \frac{d\sigma}{d\Omega} \right\rangle_{\text{unpol}} = a^2(ka)^4 \left[\frac{5}{8}(1 + \cos^2\theta) - \cos\theta \right].$$

(d) Compare the answer in (c) with the cross section when the incident plane wave is circularly polarized.

21.6 Scattering from a Molecular Rotor A linearly polarized, monochromatic plane wave scatters from a polar molecule by exerting a torque which sets the molecule into motion. Treat the molecule as an electric dipole with moment $\mathbf{p}$ and moment of inertia I. Ignore terms quadratic in the (very slow) angular velocity $\boldsymbol{\Omega}$ of the molecule and average over all orientations of $\mathbf{p}$ to show that the total scattering cross section is $\sigma_{\text{scatt}} = \mu_0^2 p^4/9\pi I^2$. Hint: A rotating dipole moment satisfies $\dot{\mathbf{p}} = \boldsymbol{\Omega} \times \mathbf{p}$.

21.7 Preservation of Polarization I A linearly polarized plane wave with electric field amplitude $\mathbf{E}_0$ is incident on a small, perfectly conducting sphere. Use the dipole moment information provided in Problem 21.5 and find the angle between the scattering wave vector $\mathbf{k}$ and the incident wave vector $\mathbf{k}_0$ where the radiated electric field points in the same direction as $\mathbf{E}_0$.

21.8 Scattering and Absorption by an Ohmic Sphere A low-frequency, plane electromagnetic wave Rayleigh scatters from a sphere with radius a and conductivity σ. Assume that the skin depth $\delta \gg a$.

(a) Find the electric dipole moment induced in the sphere by the incident wave.

(b) Calculate the absorption cross section of the sphere.

(c) Show that the optical theorem is satisfied by the absorption cross section (alone) and the electric dipole scattering amplitude.

(d) Rationalize the result of part (c) with the fact that the scattering cross section is not zero.

21.9 Scattering from a Dielectric Cylinder The symmetry axis of an infinitely long dielectric cylinder with radius a and permittivity ϵ coincides with the z-axis. A monochromatic wave with wave vector $\mathbf{k}_0$ is normally incident on the cylinder as shown below. Find the electric field everywhere if the incident wave is polarized in the z-direction.

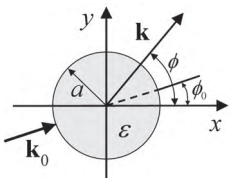

21.10 Preservation of Polarization II A monochromatic plane wave with electric field amplitude $\mathbf{E}_0$ is incident on a perfectly conducting object with an arbitrary shape. Prove that the electric field radiated in the backward direction is parallel to $\mathbf{E}_0$ in the physical optics approximation.

21.11 Scattering from a Conducting Strip A thin and infinitely long, perfectly conducting strip occupies the area $0 \le x \le w$ of the $y = 0$ plane. A monochromatic plane wave polarized along $+z$ scatters from the strip as shown below. Assume specular reflection and let $\omega = ck = ck_0$.

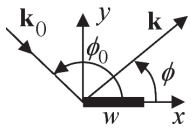

(a) Find the physical optics surface current density.

(b) Perform the z' integration in the exact vector potential produced by $\mathbf{K}_{\mathrm{PO}}(\mathbf{r}, t)$ and use the Hankel function identity,

$$i\pi H_0^{(1)}(x) = \int_{-\infty}^{\infty} d\eta \frac{\exp(i\sqrt{x^2+\eta^2})}{\sqrt{x^2+\eta^2}},$$

to show that

$$\mathbf{A}(\mathbf{r}, t) = \hat{\mathbf{z}} \frac{i\mu_0 E_0}{2Z_0} \sin\phi_0 \int_0^w dx' H_0^{(1)}(k|\boldsymbol{\rho} - \boldsymbol{\rho}'|) \exp(-ikx' \cos\phi_0) \exp(-i\omega t).$$

(c) Evaluate $\mathbf{A}(\rho, \phi)$ in the far zone and show that the two-dimensional differential cross section for scattering is

$$\frac{d\sigma}{d\phi} = \frac{2}{\pi k} \sin^2\phi_0 \frac{\sin^2\left[\frac{1}{2}kw(\cos\phi + \cos\phi_0)\right]}{(\cos\phi + \cos\phi_0)^2}.$$

Hint: Do not completely neglect the dependence of $|\boldsymbol{\rho} - \boldsymbol{\rho}'|$ on x' when approximating a phase factor in the far zone.

21.12 Physical Optics Backscattering

(a) Let S be the illuminated portion of a conductor. If $\hat{\mathbf{n}}$ is the local unit normal vector to S and $\mathbf{k} = k_0\hat{\mathbf{k}}$ is the propagation direction of the backscattered wave, show that the cross section for backscattering in the physical optics approximation is

$$\sigma_{\mathrm{R}} = \frac{k_0^2}{4\pi^2} \left| \int_S dS' \, \hat{\mathbf{k}} \cdot \hat{\mathbf{n}}' \exp(-2i\mathbf{k} \cdot \mathbf{r}') \right|^2.$$

(b) Specialize to a flat, rectangular plate with negligible thickness that lies in the $z = 0$ plane. The side parallel to the x-axis has length a and the side parallel to the y-axis has length b. If the center of the plate coincides with the origin of spherical coordinates and the plate area is A, show that

$$\sigma_{\mathrm{R}} = \frac{A^2}{\lambda^2} \cos^2\theta \left[\frac{\sin(k_0 a \sin\theta \cos\phi)}{k_0 a \sin\theta \cos\phi} \times \frac{\sin(k_0 b \sin\theta \sin\phi)}{k_0 b \sin\theta \sin\phi} \right]^2.$$

21.13 Born Scattering from a Dielectric Cube A plane wave $\mathbf{E}_0 \exp[i(\mathbf{k}_0 \cdot \mathbf{r} - \omega t)]$ scatters from a dielectric cube with volume $V = a^3$ and electric susceptibility $\chi_e \ll 1$. Two cube edges align with $\mathbf{k}_0$ and $\mathbf{E}_0$.

(a) Calculate the differential scattering cross section in the Born approximation.

(b) Show that $\sigma_{\text{Born}} \approx \frac{1}{4}k^2a^4\chi_e^2$ when $ka \gg 1$. Hint: The near-forward direction dominates the scattering when $ka \gg 1$.

(c) The weak scattering assumed by the Born approximation implies that $|\mathbf{E}_{\text{rad}}|/|\mathbf{E}_0| \ll 1$ for all $\mathbf{q}$, even when $r \approx a$. Deduce from this that the $ka \gg 1$ result of part (b) is valid only when $\sigma_{\text{Born}} \ll \chi_e a^2$.

21.14 Scattering from a Short Conducting Wire A monochromatic plane wave scatters from a perfectly conducting wire where $a \ll h$. Assume that both the propagation vector and the electric field of the incident wave lie in the y-z plane as shown below.

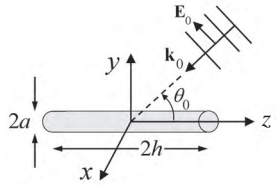

(a) In the Rayleigh limit when $k_0h \ll 1$, the scattering is dominated by a z-directed electric dipole moment $\mathbf{p} = \epsilon_0\alpha(\hat{\mathbf{z}} \cdot \mathbf{E}_0)\hat{\mathbf{z}}$. Assume an induced surface current density,

$$\mathbf{K}(z) = \frac{I_0}{2\pi a}\left[1 - (z/h)^2\right]\hat{\mathbf{z}},$$

and determine the parameter I_0 by imposing the perfect-conductor condition, $[\mathbf{E}_{\text{scatt}} + \mathbf{E}_0] \cdot \hat{\mathbf{z}} = 0$, at a single point: the origin of coordinates at the center of the wire. Specifically, calculate $\mathbf{E}_{\text{scatt}}$ from a near-zone expansion of the retarded potentials and show that

$$I_0 = \frac{-i\pi\omega h^2}{\{[\ln(2h/a) - 1][1 - \frac{1}{2}(kh)^2] + i\frac{2}{9}(kh)^3\}}\hat{\mathbf{z}} \cdot \mathbf{E}_0.$$

(b) Drop the terms of order $(k_0h)^2$ and $(k_0h)^3$ from the expression for I_0, compute the induced electric dipole moment, and use this to find the total scattering cross section.

(c) Show that the terms dropped in part (b) must be retained in the radiation zone forward scattering amplitude to satisfy the optical theorem with the cross section computed in part (b).

21.15 Absorption Cross Section for a Microscopic Object Show that $\sigma_{\text{abs}} = (\omega/c)\text{Im}\alpha$ is the frequency-dependent absorption cross section for a microscopic object (atom, molecule, or nucleus) with polarizability α.

21.16 Absorption Sum Rule for a Lorentz Oscillator A monochromatic plane wave scatters from a Lorentz atom where a bound electron obeys the classical equation of motion $\ddot{\mathbf{r}} + \gamma\dot{\mathbf{r}} + \omega_0^2\mathbf{r} = 0$. Assume that the electron displacement and damping are both very small. If $r_e = e^2/4\pi\epsilon_0 mc^2$ is the classical electron radius, show that the integrated total absorption cross section is independent of the damping constant:

$$\int_0^\infty d\omega\, \sigma_{\text{abs}}(\omega) = 2\pi^2 r_e c.$$

21.17 The Optical Theorem in Two Dimensions

(a) Integrate the differential cross sections derived in the text to find the total scattering cross sections $\sigma_\parallel$ and $\sigma_\perp$ for an infinitely long and perfectly conducting cylinder with $\mathbf{E}_{\text{inc}}$ oriented, respectively, parallel and perpendicular to the cylinder axis.

(b) In two dimensions, the scattering amplitude $\mathbf{f}(\mathbf{k}) = \mathbf{f}(k, \phi)$ is defined by the asymptotic electric field

$$\mathbf{E}_{\text{rad}}(\rho, \phi) = E_0\sqrt{\frac{i}{k}}\mathbf{f}(\mathbf{k})\frac{\exp(ik\rho)}{\sqrt{\rho}}.$$

Use the results of part (a) for either polarization to confirm that the optical theorem in two dimensions is

$$\sigma_{\text{tot}} = \frac{\sqrt{8\pi}}{k}\,\text{Im}[\hat{\mathbf{e}}_0^* \cdot \mathbf{f}(k, 0)].$$

21.18 The Optical Theorem for Pedestrians A unit-amplitude, monochromatic plane wave of a scalar field $\psi(\mathbf{r})$ scatters from an origin-centered obstacle of finite size. Apart from a factor of $\exp(-i\omega t)$, the field takes the asymptotic form

$$\psi(r, \theta, \phi) \approx \exp(ikz) + \frac{\exp(ikr)}{r} f(\theta, \phi).$$

Focus on the almost-forward direction where $\theta \ll 1$ and suppose that a flat screen with a radius $R \gg z/k$ collects the energy of the wave at a distance $z \gg R$ from the origin. Show that

$$\int_{\text{screen}} dS\,|\psi|^2 \approx \pi R^2 - \frac{4\pi}{k}\text{Im}\,f(0),$$

where $f(0)$ is the scattering amplitude evaluated on the z-axis. Use this result to argue that

$$\sigma_{\text{tot}} = \sigma_{\text{scatt}} + \sigma_{\text{abs}} = \frac{4\pi}{k}\text{Im}\,f(0).$$

21.19 Total Cross Section Sum Rule An incident plane wave $\hat{\mathbf{e}}_0 E_0 \exp[i(\mathbf{k}_0 \cdot \mathbf{r} - \omega t)]$ scatters from a target with amplitude $\mathbf{f}(\mathbf{k})$. One can prove that $\mathbf{f}(\mathbf{k}_0) \cdot \hat{\mathbf{e}}_0^*/k^2$ is a causal response function of the sort discussed in Section 18.7. Use this information to prove the wavelength sum rule,

$$\lim_{\lambda \to \infty} \text{Re}\,[\mathbf{f}(\lambda, \mathbf{k}_0) \cdot \hat{\mathbf{e}}_0^*] = \frac{1}{\pi\lambda^2}\int_0^\infty d\lambda'\,\sigma_{\text{tot}}(\lambda').$$

21.20 The Index of Refraction Let $\mathbf{E}_{\text{inc}} = \mathbf{e}_0 E_0 \exp[i(kz - \omega t)]$ be the electric field of a plane wave propagating in a homogeneous dielectric medium. The wave vector $k = nk_0 = n\omega/c$, where n is the index of refraction of the medium. Suppose that the number density of scatters increases from N to $N + \delta N$ in a thin layer of the medium between $z = 0$ and $z = \delta t$. Because δt is infinitesimal, $\mathbf{E}_{\text{inc}}$ scatters once from every extra atom in the layer. Therefore, if the atomic scattering amplitude is $\mathbf{f}(\theta, \phi)$, the extra electric field produced at the distant observation point $z \gg \delta t$ is

$$\mathbf{E}_{\text{rad}}(z) = \delta N E_0 \delta t \int_{\text{layer}} d^2 r\,\frac{\exp(ikR)}{R}\mathbf{f}(\theta, \phi).$$

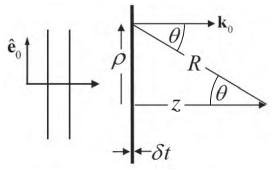

(a) Change variables to $\eta = R/z$, integrate by parts, and compare the original integral to the new integral in the limit $kz \gg 1$. Note that $\mathbf{f}(0) \equiv \mathbf{f}(\theta = 0, \phi)$ does not depend on ϕ and establish that

$$\mathbf{E}_{\text{rad}}(z) = \frac{2\pi i}{k}\delta N E_0 \delta t \exp(ikz)\,\mathbf{f}(0) \qquad kz \gg 1.$$

(b) Construct $\mathbf{E}(z) = \mathbf{E}_{\text{inc}}(z) + \mathbf{E}_{\text{rad}}(z)$ from the results of part (a) and argue that your expression remains valid at $z = \delta t$. Derive from this fact an expression for $\delta k/\delta N$, the change in wave vector induced by

the density perturbation. Integrate and conclude that the index of refraction of the unperturbed medium satisfies

$$n^2 = 1 + \frac{4\pi N}{k_0^2}\hat{\mathbf{e}}_0^* \cdot \mathbf{f}(0).$$

21.21 Radiation Pressure from Scattering An object scatters an incident plane wave with $\mathbf{E}_{\text{inc}}(\mathbf{r}, t) = \hat{\mathbf{e}}_0 E_0 \exp[i(\mathbf{k}_0 \cdot \mathbf{r} - \omega t)]$. Use the Maxwell stress tensor formalism to show that the time-averaged force on the object can be written in terms of the incident wave intensity I_{inc}, the total cross section σ_{tot}, and the differential cross section for scattering $d\sigma_{\text{scatt}}/d\Omega$ as

$$\langle \mathbf{F} \rangle = \frac{I_{\text{inc}}}{c}\left[\sigma_{\text{tot}}\hat{\mathbf{k}}_0 - \int d\Omega\, \hat{\mathbf{r}}\frac{d\sigma_{\text{scatt}}}{d\Omega}\right].$$

The projection of this force on the direction $\hat{\mathbf{k}}_0$ is often called the radiation pressure due to scattering. Hint: Integrate the stress tensor over the surface of an enormous sphere in the radiation zone.

21.22 A Backscatter Theorem Theorem: A monochromatic plane wave incident on a body with $\epsilon(\mathbf{r}) = \mu(\mathbf{r})$ produces zero scattered field intensity in the far zone in the backward direction if the direction of incidence is an axis of symmetry where rotation by 90° leaves the body unchanged. To prove this,

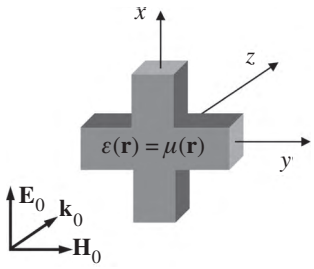

(a) Begin with the Maxwell equations for matter with a spatially varying permittivity and permeability. Show that $\mathbf{E}(\mathbf{r})$ and $\mathbf{H}(\mathbf{r})$ satisfy the same generalized wave equation when $\epsilon(\mathbf{r}) = \mu(\mathbf{r})$.

(b) Let $\mathbf{E}^{\text{scatt}}$ be the exact electric field produced by the body. Show that

$$\mathbf{H}^{\text{scatt}}(x, y, z) = -E_y^{\text{scatt}}(y, -x, z)\hat{\mathbf{x}} + E_x^{\text{scatt}}(y, -x, z)\hat{\mathbf{y}} + E_z^{\text{scatt}}(y, -x, z)\hat{\mathbf{z}}.$$

(c) Use the results of part (a), part (b), and a consideration of the Poynting vector in the radiation zone to prove the theorem.

21.23 The Angular Spectrum of Plane Waves in Two Dimensions Consider time-harmonic electromagnetic fields in the domain $z \geq 0$ of the form

$$\mathbf{E}(x, z \geq 0, t) = \mathbf{E}(x, z, \omega)\exp(-i\omega t) \qquad \mathbf{B}(x, z \geq 0, t) = \mathbf{B}(x, z, \omega)\exp(-i\omega t).$$

(a) Let $\hat{\mathbf{y}} \cdot \mathbf{E}_{\text{TE}}(x, z = 0, t = 0) = \bar{E}_y(x)$. Determine the scalar function $\Lambda_{TE}(k_x)$ and the vector function $\mathbf{\Gamma}_{TE}(k_x)$ so that

$$\mathbf{E}_{TE}(x, z, \omega) = \hat{\mathbf{y}} \int_{-\infty}^{\infty} \frac{dk_x}{2\pi}\, \Lambda_{TE}(k_x)\exp(i\,\mathbf{k} \cdot \mathbf{r})$$

$$\mathbf{B}_{TE}(x, z, \omega) = \int_{-\infty}^{\infty} \frac{dk_x}{2\pi}\, \mathbf{\Gamma}_{TE}(k_x)\exp(i\,\mathbf{k} \cdot \mathbf{r})$$

solve Maxwell's equations in free space. The wave vector $\mathbf{k} = \hat{\mathbf{x}}\,k_x + \hat{\mathbf{z}}\,k_z$ is two-dimensional. Explain why there is no integral over k_z.

(b) Let $\hat{\mathbf{x}} \cdot \mathbf{E}_{\mathrm{TM}}(x, z = 0, t = 0) = \bar{E}_x(x)$. Determine the scalar function $\Lambda_{TM}(k_x)$ and the vector function $\Gamma_{TM}(k_x)$ so that

$$\mathbf{B}_{TM}(x, z, \omega) = \hat{\mathbf{y}} \int_{-\infty}^{\infty} \frac{dk_x}{2\pi c} \frac{k_0}{k_z} \Lambda_{TM}(k_x) \exp(i\,\mathbf{k} \cdot \mathbf{r})$$

$$\mathbf{E}_{TM}(x, z, \omega) = \int_{-\infty}^{\infty} \frac{dk_x}{2\pi} \Gamma_{TM}(k_x) \exp(i\,\mathbf{k} \cdot \mathbf{r})$$

solve Maxwell's equations in free space. The factor $k_0 = \omega/c$.

(c) Represent a general $z \geq 0$ field as $\mathbf{E} = \mathbf{E}_{TE} + \mathbf{E}_{TM}$ and $\mathbf{B} = \mathbf{B}_{TE} + \mathbf{B}_{TM}$. If $\mathbf{S}$ is the Poynting vector, show that the time-averaged power transmitted down the z-axis is

$$P_z = \int_{-\infty}^{\infty} dx \; < \mathbf{S} \cdot \hat{\mathbf{z}} >= \frac{1}{4\pi} \sqrt{\frac{\epsilon_0}{\mu_0}} \int_{-k_0}^{k_0} dk_x \left\{ |\Lambda_{TM}|^2 \frac{k_0}{k_z} + |\Lambda_{TE}|^2 \frac{k_z}{k_0} \right\}.$$

What is the physical origin of the limits of integration on the k_x integral?

21.24 Weyl's Identity This problem outlines a contour integration method to prove that

$$\frac{\exp(ik_0 r)}{4\pi r} = \frac{i}{8\pi^2} \int \frac{d^2 k_\perp}{k_z} \exp(i\mathbf{k}_\perp \cdot \mathbf{r}_\perp + ik_z|z|),$$

where

$$k_z = \begin{cases} \sqrt{k_0^2 - k_x^2 - k_y^2} & k_x^2 + k_y^2 \leq k_0^2, \\ i\sqrt{k_x^2 + k_y^2 - k_0^2} & k_x^2 + k_y^2 \geq k_0^2. \end{cases}$$

(a) The left side of the Weyl identity is the free-space Green function, $G_0(\mathbf{r})$, which satisfies $(\nabla^2 + k_0^2)G_0(\mathbf{r}) = -\delta(\mathbf{r})$. Fourier transform this differential equation and show that

$$G_0(\mathbf{r}) = \frac{1}{(2\pi)^3} \int d^3 k \, \frac{\exp(i\mathbf{k} \cdot \mathbf{r})}{k^2 - k_0^2}.$$

(b) Use contour integration to perform the integral over k_z in part (a). Assume that k_0 has a small positive imaginary part to establish the location of the poles and to decide how to close the contour.

21.25 Radiation from an Open Waveguide The $a \times b$ rectangular aperture of an infinite conducting plane is illuminated by the TE_{10} mode of a rectangular waveguide with the same cross sectional shape as the aperture. Evaluate the radiated electric field at the point (r, θ, ϕ) with respect to an origin at the center of the aperture using Kirchoff's approximation to the Fraunhofer-Smythe formula (21.98).

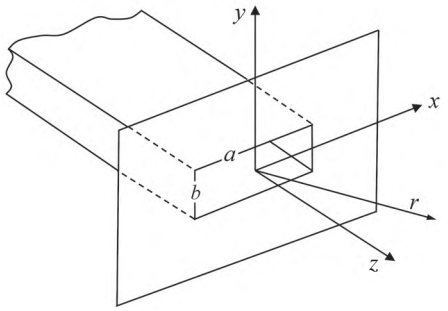

21.26 Diffraction from a Slit A plane wave propagating in the $+x$-direction with electric field $\mathbf{E}_0$ strikes a thin metal screen at $x = 0$ and diffracts from a long and narrow horizontal slit (width a) cut out of the screen. The

scattering vector $\mathbf{k}$ lies in the x-y plane (perpendicular to the long direction of the slit) at an angle ϕ from the forward direction. Evaluate Smythe's formula (21.90) using Kirchoff's approximation and the far-field limit of the free-space Green function in two dimensions, $G_0^{(2)}(\boldsymbol{\rho}, \boldsymbol{\rho}') = (i/4)H_0^{(1)}(k|\boldsymbol{\rho} - \boldsymbol{\rho}'|)$, to show that the diffracted electric field is

$$\mathbf{E}(\rho, \phi) = -\frac{a}{2}\mathbf{k} \times (\hat{\mathbf{x}} \times \mathbf{E}_0)\sqrt{\frac{2}{\pi k\rho}}\exp[i(k\rho - \pi/4)]\frac{\sin(\frac{1}{2}ka\sin\phi)}{\frac{1}{2}ka\sin\phi}.$$

21.27 Diffraction of a Beam by a Large Aperture

(a) Consider the electric field diffracted by a circular aperture of radius a using a Kirchoff approximation where $\mathbf{E}_{\text{inc}} = E_0\exp(-\rho^2/w^2)\hat{\mathbf{y}}$ in the plane of the aperture. Show that the far-zone field still has a Gaussian profile when the beam waist $w \ll a$.

(b) Repeat the calculation for a square aperture with side length a in the same limit and compare to part (a).

21.28 Effective Aperture Dipoles I Let $z = 0$ be a perfect conductor except for an aperture whose size is very small compared to the wavelength of a plane wave incident from $z < 0$. Perform a multipole expansion of the far-zone limit of Smythe's formula and find the effective electric and magnetic dipole moments of the aperture in the terms of $\mathbf{E}_\parallel$, the component of the exact electric field in the plane of the aperture. Are your results consistent with Figure 21.21?

21.29 Effective Aperture Dipoles II A monochromatic plane wave with fields $\mathbf{E}_0$ and $\mathbf{B}_0$ scatters from a thin conducting disk of radius a. In the long-wavelength limit, the scattered field is described by electric and magnetic dipole radiation fields with moments

$$\mathbf{p}_{\text{d}} = -\frac{16}{3}a^3\epsilon_0\hat{\mathbf{n}} \times (\hat{\mathbf{n}} \times \mathbf{E}_0) \qquad \text{and} \qquad \mathbf{m}_{\text{d}} = -\frac{8}{3\mu_0}a^3(\hat{\mathbf{n}} \cdot \mathbf{B}_0)\hat{\mathbf{n}}.$$

The unit vector $\hat{\mathbf{n}}$ points in the direction of the incident wave propagation vector when the latter is normal to the plane of the disk. Use Babinet's principle to deduce the effective dipole moments which characterize the diffracted field when a circular hole of radius a in a flat conducting plane is illuminated by a plane wave with aperture fields $\mathbf{E}_{\text{a}}$ and $\mathbf{B}_{\text{a}}$. Do not assume normal incidence for the diffraction problem.

21.30 Kirchhoff's Approximation for Complementary Scatterers A monochromatic plane wave polarized along $\hat{\mathbf{y}}$ is normally incident from $z < 0$ onto a two-dimensional conducting scatterer confined to the $z = 0$ plane. Use Kirchoff's approximation but do *not* use the Fraunhofer approximation.

(a) Let the scatterer be a conducting disk of radius a. Find $\mathbf{E}_{\text{disk}}(0, 0, z > 0)$.

(b) Let the scatterer be an infinite conducting sheet with a circular aperture of radius a centered on the z-axis. Find $\mathbf{E}_{\text{aperture}}(0, 0, z > 0)$.

(c) Confirm that $\mathbf{E}_{\text{aperture}}(0, 0, z > 0) = \mathbf{E}_{\text{inc}} - \mathbf{E}_{\text{disk}}(0, 0, z > 0)$. Explain why Babinet's principle is *not* the reason this is true.